Exclusive Electro-Disintegration of ^{3}He at high Q^2:
II. Decay Function Formalism

M.M. Sargsian, T.V. Abrahamyan

Department of Physics, Florida International University, Miami, Florida 33199

M.I. Strikman

Department of Physics, Pennsylvania State University, University Park, PA

L.L. Frankfurt

Department of Nuclear Physics, Tel Aviv University, Tel Aviv, Israel

February 9, 2008

Abstract

Based on the theoretical framework of generalized eikonal approximation we study the two-nucleon emission reactions in high Q^2 electro-disintegration of ^3He. Main aim is to investigate those features of the reaction which can be unambiguously identified with the short range properties of the ground state nuclear wave function. To evaluate the differential cross section we work in the formalism of the decay function which characterizes the property of the ground state wave function as well as the decay properties of final two nucleon spectator system. Our main motivation here is to explore the accessibility of two– and three–nucleon short range correlations in ^{3}He as well as to isolate unambiguously single and double rescattering processes in the reaction dynamics. Our analysis allowed us also to identify new approaches for investigating the role of the practically unknown three-nucleon forces in the ground state wave function of ^3He.

I. INTRODUCTION

In this work we study high Q^2 ($4 \gtrsim Q^2 \gtrsim 1$ GeV^2) exclusive $^3He(e, e'NN)N$ reactions in which one nucleon in the final state can be clearly identified as a knocked-out nucleon which carries practically all of the momentum of the virtual photon.

In the part-I of the present work [1] we calculated the scattering amplitude of this type of reactions within the generalized eikonal approximation (GEA), in which one expresses the scattering amplitude through the sum of the diagrams corresponding to the n'th order rescattering of the knocked-out nucleon with the residual nucleons in the nucleus. In

Ref. [1] we evaluated each diagram based on the effective Feynman diagram rules derived within the GEA [2,3]. The manifestly covariant nature of Feynman diagrams allowed us to preserve both the relativistic dynamics and the kinematics of the rescattering while identifying the low momentum nuclear part of the amplitude with the nonrelativistic nuclear wave function. Such an approach allows us to account for the internal motion of residual target nucleons in the rescattering amplitude as well as finite excitation energies of residual nuclear system. These features of the GEA are crucial in describing electro-production reactions aimed at the study of short-range nuclear properties since these configurations are characterized by non-negligible values of bound nucleon momenta and excitation energies. The study of short-range nucleon correlations is the main goals of the present work. With short-range correlations we identify those interactions between bound nucleons that generate nucleon momenta exceeding the characteristic Fermi momentum of the nuclear system, $k_F \approx 250$ MeV/c. This encompasses interactions due to the short-distance repulsive core and the short to medium-distance tensor interactions of NN system as well as possible three-nucleon interactions which can have both short and medium distance terms.

Working in the virtual nucleon framework [1] one describes the reaction in the Lab frame relating all non-nucleonic degrees of freedom effectively to the off-shellness of the knocked–out (virtual) nucleon in the nucleus. For recent analysis of similar reaction with two proton emission in the final state see Ref. [5]. In calculation of the differential cross section of the reaction we utilize the kinematics of high Q^2 quasielastic scattering with knocked-out nucleon identified unambiguously in the final state of the reaction. This allows us to employ the decay function formalism in which the eA cross section of the reaction can be represented through the convolution of the off-shell electron–bound nucleon cross section and the decay function which characterizes the ground state properties of the nucleus as well as the decay of the spectator state in the final state of the reaction.

The paper is organized as follows: In Sec. II we summarize briefly the reaction, specifics of the kinematics and general form of the differential cross section. In Sec.III we elaborate the decay function formalism and derive the expression for the decay function both for plane wave and distorted wave impulse approximations. For the latter case one obtains the expression based on GEA calculation of Ref. [1]. In Sec. IV the numerical analysis of both semi-inclusive $(e, e'N)$ and exclusive $(e, e'NN)$ reactions are presented. In these calculations as an input we use Bochum group's calculation of ground state ^3He wave function [11], SAID group's parameterization of low-to-intermediate energy NN scattering amplitudes [12] as well as our updated parameterization of the high energy small angle NN scattering amplitude [13]. The main focus in the numerical analysis is the study of two- and three- nucleon short range correlations (SRCs) and isolation of the effects associated with single and double rescattering of the knocked-out nucleon off residual nucleons in the nucleus. We observe significant sensitivity of the decay function to the configurations characteristic to the short-range two- and three-nucleon correlations in the nucleus. The $(e, e'NN)$ reaction provides also an ideal testing ground for single and double rescattering processes, which could play a crucial role for studies of color coherence phenomena in hard exclusive nuclear reactions. Our calculations allowed us also to identify kinematics which could provide unprecedented access to the three nucleon forces in ^3He. Section V summarizes our results.

II. REACTION, KINEMATICS AND CROSS SECTION

We are studying the reaction:

$$e +^3 He \rightarrow e' + N_f + N_{r2} + N_{r3} \tag{1}$$

where e and e' are the initial and scattered electrons with four-momenta k_e and k'_e respectively. The ^{3}He nucleus has a four-momentum P_A. N_f, N_{r2} and N_{r3} correspond to knocked-out and two recoil nucleons with four-momenta p_f, p_{r2} and p_{r3} respectively. We define also the four-momentum of the virtual photon $q = (q_0, \mathbf{q}, 0_\perp) \equiv k_e - k_{e'}$ with $Q^2 = -q^2$. The z direction is chosen parallel to $\mathbf{q}$ and the scattering plane is the plane of the $\mathbf{q}$ and $\mathbf{k_{e'}}$ vectors. The missing momentum of the reaction is defined as: $\mathbf{p_m} = \mathbf{p_f} - \mathbf{q}$.

In numerical estimations we will focus on the kinematic region:

$$\text{(a)} \ 4 \geq Q^2 \geq 1\text{GeV}^2; \quad \text{(b)} \ \mathbf{p_f} \approx \mathbf{q}, \tag{2}$$

which allows us to identify N_f as a knocked-out nucleon. Furthermore, we will do numerical investigations for recoil, $\mathbf{p_{r2}}$, $\mathbf{p_{r3}}$ and missing $\mathbf{p_m}$ momenta covering the region of up to $700 - 800$ MeV/c (and 1 GeV/c for the kinematics dominated by the double rescattering). This exceeds the kinematic domain of $\leq 400 - 500$ MeV/c, within which the GEA and virtual nucleon approximation can be reliably applied [1]. However, the expectation of the smooth transition to the relativistic region for the main properties of the decay function (see e.g. [6]) gives some validity to our exploratory studies in the region of ≥ 500 MeV/c. The properties we consider are the correlation relations between missing momentum/energy and momenta of the recoil nucleons, relative strength of 2N and 3N correlations as well as signatures identified with the single and double rescattering of knocked-out nucleon off spectator nucleons in the target.

A. Cross Section

In numerical calculations we restrict ourselves by consideration of unpolarized three-body electro-disintegration reaction of Eq.(1).

The differential cross section of reaction (1) in which no polarizations are fixed is given by

$$d^{12}\sigma = \frac{1}{4j_A}(2\pi)^4\delta^4(k_e + P_A - k'_e - p_f - p_{r2} - p_{r3})\frac{1}{4}A \cdot \sum_{nucleons}\sum_{spins}|M_{fi}|^2$$
$$\frac{d^3k'_e}{(2\pi)^32E'_e}\frac{d^3p_f}{(2\pi)^32E_f}\frac{d^3p_{r2}}{(2\pi)^32E_{r2}}\frac{d^3p_{r3}}{(2\pi)^32E_{r3}} \ , \tag{3}$$

where $j_A = \sqrt{(k_eP_A)^2 - m_e^2M_A^2}$. Here we sum over final and average over initial spins. The factor $1/4$ comes from the averaging over the initial polarizations of the electron and the nucleus. Since one of the recoil nucleons is not observed, one eliminates this degree of freedom by integrating over d^3p_{r3}. Thus integrated differential cross section is

$$d^9\sigma = \frac{1}{4j_A}(2\pi)^4\delta(E_e + M_A - E'_e - E_f - E_{r2} - E_{r3})\frac{1}{4}A \cdot \sum_{nucleons}\sum_{s_e,s_A}\sum_{s_{e'},s_f,s_{r2},s_{r3}}|M_{fi}|^2$$
$$\frac{d^3k'_e}{(2\pi)^32E'_e}\frac{d^3p_f}{(2\pi)^32E_f}\frac{d^3p_{r2}}{(2\pi)^32E_{r2}}\frac{1}{(2\pi)^32E_{r3}} \ , \tag{4}$$

where $\mathbf{p_{r3}} = \mathbf{k_e} - \mathbf{k'_e} - \mathbf{p_f} - \mathbf{p_{r2}}$. In Eqs. (3) and (4) the transition matrix, M_{fi}, represents the convolution of the electron and nuclear currents, in which the nuclear current within GEA [1] represents the sum of the IA, single and double rescattering amplitudes,

$$M_{fi} = -4\pi\alpha \frac{1}{q^2} j^e_\mu \cdot \left(A^\mu_0 + A^\mu_1 + A^\mu_2 \right), \tag{5}$$

where A_0, A_1 and A_2 are derived in Ref. [1] and represent impulse approximation, single and double rescattering amplitudes respectively. Their final expressions are given in Eqs.(11), (21) and (27) of Ref. [1] respectively. Note that IA corresponds to the impulse approximation contribution in which the pair distortion effects due to interaction of two outgoing recoil nucleons are taken into account.

III. NUCLEAR DECAY FUNCTION FORMALISM

In description of semi-exclusive $(e, e'N)$ reactions it is conventional to introduce a spectral function, $S^N(E_m, \mathbf{p_m})$, which in the impulse approximation picture describes the probability of finding a struck-nucleon in the nucleus initially having missing momentum $\mathbf{p_m}$ and missing energy $E_m = q_0 - T_f - \frac{p^2_m}{2(A-1)m}$. The missing energy characterizes the excitation energy of the final $A - 1$ system. We generalize this approach for the case of the exclusive reaction in (1), as well as for any semi-exclusive reactions involving two-nucleon emission by introducing a nuclear decay function which can be formally defined as [6]:

$$D^N(\mathbf{p_m}, E_m, \mathbf{p_{r2}}) = \sum_f \left| \langle A - 1 | a^\dagger(\mathbf{p_{r2}}) a(\mathbf{p_m}) | \Psi_A \rangle \right|^2 \delta(E_m - (\epsilon^f_{A-2} + T_{r2} - \epsilon_A - \frac{p^2_m}{2(A-1)m})), \tag{6}$$

where one sums over the states, f, of $A - 2$ residual nucleus and $\epsilon^f_{A-2} = E^f_{A-2} - (A-2)m$, where E^f_{A-2} is the total energy of $A - 2$ state. It follows from this definition that the decay function characterizes the joint probability to find a struck nucleon in the nucleus with momentum $\mathbf{p_m}$, missing energy E_m and the recoil nucleon with momentum $\mathbf{p_{r2}}$ in the decay product of the residual $A - 1$ nucleus. Note that for $A \geq 4$, Eq.(6) assumes the sum over all possible (bound and continuum) $(A - 2)$ substates, provided the total excitation energy of $A - 1$ final state is E_m. The general properties of the decay function are discussed in [6] where the qualitative features are studied within the two-nucleon correlation model. The following sum rule and normalization condition follow from Eq.(6):

$$\int d^3p_{r2} D^N(\mathbf{p_m}, E_m, \mathbf{p_{r2}}) = S^N(E_m, \mathbf{p_m});$$

$$\sum_N \int dE_m d^3p_m S^N(E_m, \mathbf{p_m}) = 1. \tag{7}$$

Within the impulse approximation the cross section of the reaction with two-nucleon emission can be expressed through the decay function as follows:

$$\frac{d\sigma}{dE'_e d\Omega'_e d^3p_f d^3p_{r2}} = \frac{j_N}{j_A} \cdot A \sum_N \sigma_{eN}(p_f, k_e, k'_e) \cdot D^N(\mathbf{p_m}, E_m, \mathbf{p_{r2}}), \tag{8}$$

4

where $E_m = T_{r2} + T_{r3} + |\epsilon_A| - T_{A-1}$, with T_{A-1} being the kinetic energy of the center mass of the residual $A-1$ system. j_N is the flux calculated for the moving nucleon with momentum $\mathbf{p_m}$, and σ_{eN} represents the cross section of electron - off-shell nucleon scattering[1].

Using the derivations from Sec.IIIa of Ref. [1] it is straightforward to calculate the decay function of reaction (1). According to Eq.(11) of Ref. [1] and Eq.(4) one obtains:

$$D^N(\mathbf{p_m}, E_m, \mathbf{p_{r2}}, t_{r2}) = \frac{1}{2} \sum_{s_A, s_m, s_{r2}, s_{r3}} \left| \sum_{s_2, s_3} \sum_{t_2, t_3} \int d^3 p_{23} \Psi_{NN}^{\dagger p_{r23}, s_{r2}, t_{r2}; s_{r3}, t_{r3}}(p_{23}, s_2, t_2; s_3, t_3) \right.$$

$$\left. \times \Psi_A^{s_A}(p_m, s_m, t_m; p_2, s_2, t_2; p_3, s_3, t_3) \right|^2 \cdot \delta(E_m - T_{r2} - T_{r3} - |\epsilon_A| + \frac{p_m^2}{4m}). \tag{9}$$

Note that hereafter we use the ground state wave Ψ^{s_A} normalized to A.

To understand the role of the pair distortion in the final state of the residual nucleus we will compare D^N with the PWIA version of the decay function (D_{PWIA}^N), which corresponds to retaining the plane wave part of the residual NN system's wave function, Ψ_{NN} in Eq.(12) of Ref. [1].

We also can generalize the definition of the decay function to include the single and double rescatterings of the knock-out nucleon with residual nucleons. Such a generalization usually is meaningful within an approximation in which electromagnetic current of knocked-out nucleon is factorized from rescattering integrals of Eqs.(21) and (27) of Ref. [1]. Two conditions should be met in order for this factorization to be justified:

- First, one should be able to neglect the charge-exchange part of the amplitude for high energy small angle NN rescatterings. This follows, first, from the fact that at sufficiently high energies the energy dependence of the small angle hadronic scattering amplitude scales as $\sim s_{NN}^{J-1}$, where J corresponds to the spin of the exchanged particle [9]. Since, at energies considered, charge-exchange requires predominantly spin-0 exchange in the t-channel as compared to spin-one exchange in the diagonal channel, one expects strong s suppression of the charge-exchange amplitude as compared to the elastic NN amplitude. Analysis of the existing data on NN scattering demonstrates (see e.g. [10]) that starting at $Q^2 \geq 2$ GeV^2 the charge-exchange part amounts only a third of the forward scattering NN amplitude and decreases linearly with an increase of Q^2. Moreover, this contribution is further suppressed due to the fact that the charge-exchange amplitude is predominantly real and does not interfere with the dominant part of the FSI amplitudes which are predominantly imaginary. Taking into account also the larger slope factor of the t dependence of charge-exchange amplitude as compared to the forward scattering, one estimates only a few percent overall contribution to the NN rescattering amplitude at $Q^2 \geq 2$ GeV^2. This contribution decreases sharply with an increase of Q^2.

- Secondly, the transfered momentum, q, should be large enough that one can neglect the k, k_2 and k_3 dependencies in the electromagnetic current in Eqs.(21) and (27) of

---

[1]Note, that in some cases σ_{eN} is defined without the flux factor (see e.g. [7]). In these cases factor $\frac{j_N}{j_A}$ should not be included in Eq.(8).

Ref. [1]. Such an approximation is justified by the kinematic condition of Eq.(2) and by the fact that the characteristic average momenta transferred during NN rescattering are restricted by the slope of the exponent in Eq.(A2) of Ref. [1], i.e. $\langle k^2 \rangle, \langle k_2^2 \rangle, \langle k_3^2 \rangle \leq \frac{2}{B} \sim 250$ (MeV/c)^2.

Keeping only the diagonal part in the NN rescattering amplitude and factorizing the electromagnetic current of knocked-out nucleon, we arrive at an expression similar to Eq.(8) in which we refer D as a decay function calculated within the distorted wave impulse approximation (DWIA), D_{DWIA}. Based on Eqs.(11,21,27) of Ref. [1], for D_{DWIA} one obtains:

$$
D_{DWIA}^N(Q^2, \mathbf{p_m}, E_m, \mathbf{p_{r2}}, t_{r2}) = \frac{1}{2} \sum_{s_A, s_m, s_{r2}, s_{r3}}
$$

$$
\Bigg| \sum_{s_2,s_3} \sum_{t_2,t_3} \Bigg\{ \int d^3 p_{23} \Psi_{NN}^{\dagger p_{r23}, s_{r2}, t_{r2}; s_{r3}, t_{r3}}(p_{23}, s_2, t_2; s_3, t_3) \Psi_A^{s_A}(p_m, s_m, t_f; p_2, s_2, t_2; p_3, s_3, t_3)
$$

$$
- \frac{1}{2} \int \frac{d^3 k \, d^3 p_{23}}{(2\pi)^3} \Psi_{NN}^{\dagger p_{r23}, s_{r2}, t_{r2}; s_{r3}, t_{r3}}(p_{23}, s_2, t_2; s_3, t_3) \frac{1}{\Delta^0 - k_z + i\varepsilon}
$$

$$
\times \Bigg[\chi_1(s_2^{NN}) f_{NN}^{t_f, t_2 | t_f, t_2}(k_\perp) \cdot \Psi_A^{s_A}\left(p_m + k, s_m, t_f; -\frac{p_m}{2} + p_{23} - k, s_2, t_2; -\frac{p_m}{2} - p_{23}, s_3, t_3\right)
$$

$$
+ \chi_1(s_3^{NN}) f_{NN}^{t_f, t_3 | t_f, t_3}(k_\perp) \cdot \Psi_A^{s_A}\left(p_m + k, s_m, t_f; -\frac{p_m}{2} + p_{23}, s_2, t_2; -\frac{p_m}{2} - p_{23} - k, s_3, t_3\right) \Bigg]
$$

$$
+ \frac{1}{4} \int d^3 p_{23}' \frac{d^3 k_3}{(2\pi)^3} \frac{d^3 k_2}{(2\pi)^3} \Psi_{NN}^{\dagger p_{r23}, s_{r2}, t_{r2}; s_{r3}, t_{r3}}(p_{23}', s_2, t_2; s_3, t_3) \cdot f_{NN}^{t_3, t_f | t_3, t_f}(k_{3\perp}) f_{NN}^{t_2, t_f | t_2, t_f}(k_{2\perp})
$$

$$
\times \Bigg[\frac{\chi_2(s_{b3}^{NN})}{\Delta_3 - k_{3z} + i\varepsilon} \frac{\chi_1(s_{a2}^{NN})}{\Delta^0 - k_{2z} - k_{3z} + i\varepsilon} + \frac{\chi_2(s_{b2}^{NN})}{\Delta_2 - k_{2z} + i\varepsilon} \frac{\chi_1(s_{a3}^{NN})}{\Delta^0 - k_{2z} - k_{3z} + i\varepsilon} \Bigg]
$$

$$
\times \Psi_A^{s_A}\left(p_m + k_3 + k_2, s_m, t_f; -\frac{p_m}{2} - k_2 + p_{23}', s_2, t_2; -\frac{p_m}{2} - k_3 - p_{23}', s_3, t_3\right) \Bigg\} \Bigg|^2
$$

$$
\times \delta\left(E_m - T_{r2} - T_{r3} - |\epsilon_A| + \frac{p_m^2}{4m}\right). \tag{10}
$$

Further in the text we will refer D_{DWIA} also as D_{IA+FSI} [2].

<h3 style="text-align:center">IV. NUMERICAL RESULTS</h3>

In our numerical analysis we use the following inputs:

- **Ground State Wave function:** We use the ^3He ground state wave functions calculated by the Bochum group [11] solving Faddeev equation for different sets of realistic NN potentials. Authors in Ref. [11] consider also the different models of 3N forces with the main motivation to describe the binding energy of the $A = 3$ system.

---

[2]The cases in which only a single rescattering is considered we refer to as IA+FSI1.

- **Pair Distortion:** To estimate the reinteraction of two outgoing slow nucleons in Eq.(12) of Ref. [1] we use the SAID group's parameterization of the NN scattering amplitudes based on the partial wave analysis of the NN scattering data [12]. This parameterization successfully describes the NN scattering data at a low to intermediate momentum range ($p_{LAB} \leq 1.3/3$ GeV/c for pn/pp scattering).

- **FSI:** To estimate the single and double rescattering contributions in the total scattering amplitude, we use the following conventional parameterization for high energy small angle NN scattering:

$$f^{NN} = \sigma_{tot}^{NN}(s)(i + \alpha^{NN}(s))e^{\frac{B^{NN}(s)}{2}t}\delta^{h_1,h_1'}\delta^{h_2,h_2'}, \tag{11}$$

where we parameterized [13] σ_{tot}^{NN}, $\alpha^{NN}(s)$ and $B^{NN}(s)$ for both pn and pp scattering. We use practically all published data on small angle nucleon-nucleon scattering.

In performing the numerical integrations in Eqs.(21) and (27) of Ref. [1] we represent the knocked-out nucleon propagator in the integral as a sum of the pole and principal value (P.V.) terms

$$\frac{1}{\Delta - k_z + i\epsilon} = -i\pi\delta(\Delta - k_z) + P.V.\frac{1}{\Delta - k_z}, \tag{12}$$

where k_z and Δ characterize the transfered longitudinal momenta due to rescattering. Note that strictly speaking one can use the parameterization of the free (on-shell) NN scattering amplitude in Eq.(11) for the pole term of Eq.(12) only. For the P.V. term, the NN rescattering amplitude is off-shell. However, we use the parameterization in Eq.(11) for P.V. term too since, in the kinematics of interest, the P.V. term is only a small correction as compared to the pole contribution of Eq.(12).

In the following numerical analyzes our main goal is to identify the strategies which are best suited for investigation of two- and three- nucleon short range correlations.

For **two nucleon** correlations we are particularly interested in isolation and studies of the following configurations:

- **Type 2N-I** correlations from which a nucleon is knocked-out by virtual photon, while the third nucleon moves in the mean field of 2N SRC Fig.1(a). For the idealized case of third nucleon at rest one obtains a correlation relation:

$$E_m^{(2N-I)} = \sqrt{m^2 + p_m^2} - m - T_{A-1}, \tag{13}$$

where $T_{A-1} = \sqrt{4m^2 + p_m^2} - 2m$. Note that although we apply the approximation, $p^2/m^2 \ll 1$ in calculation of the scattering amplitudes, we still use the relativistic form of the kinetic energy to preserve the relativistic kinematics.

- **Type 2N-II** correlations in which virtual photon strikes a third isolated nucleon while 2N SRC breaks up at the final state of the reaction, Fig.1(b). In this case the expected correlation between E_m and $\mathbf{p_{r2}} \approx -\mathbf{p_{r3}}$ for the case of $p_m \approx 0$ is:

$$E_m^{(2N-II)} = \sqrt{m^2 + p_{r2}^2} + \sqrt{m^2 + p_{r3}^2} - 2m \tag{14}$$
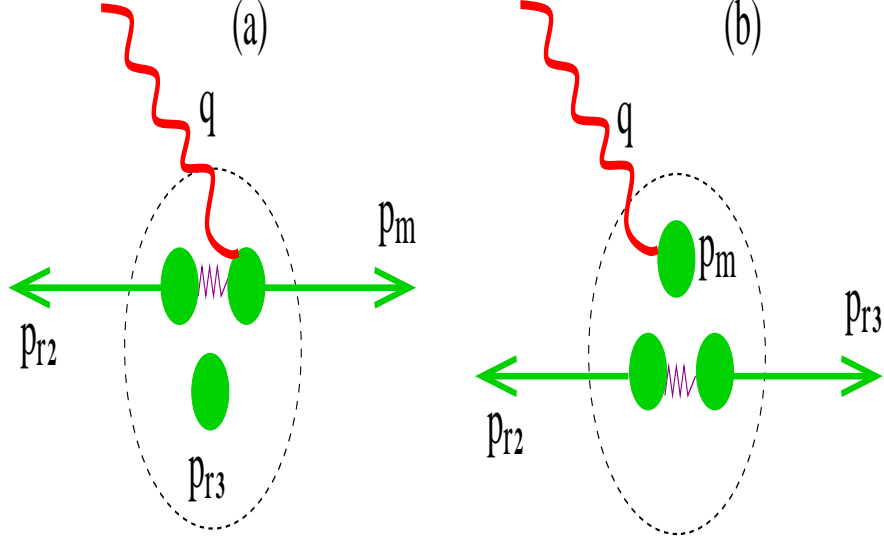
7

FIG. 1. (Color online) Definition of type 2N-I (a) and type 2N-II (b) correlations.
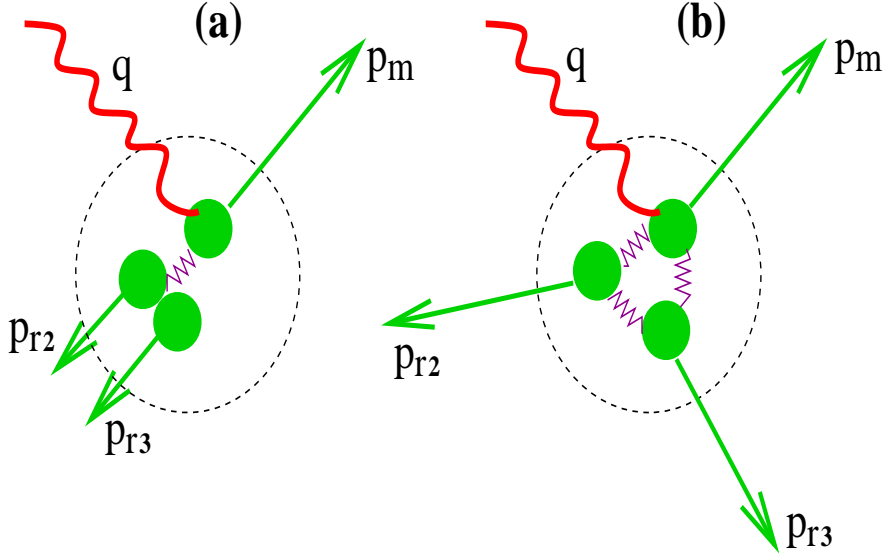

FIG. 2. (Color online) Definition of type 3N-I (a) and type 3N-II (b) correlations.

For **three nucleon** correlations we focus on two particular situations:

- **Type 3N-I** correlations, in which case the high missing momentum of the knocked-out nucleon is balanced by two nucleons which share almost equally the missing momentum p_m, Fig.2(a). This corresponds to the minimal missing mass of recoil 2N system with missing energy:

$$E_m^{(2N-I)} \approx |\epsilon_A|. \tag{15}$$

- **Type 3N-II** correlations, in which case the nucleon is knocked-out from the symmetric configurations where all three nucleons have the same momentum p_m, Fig.2(b). This corresponds to a significantly higher value of E_m as compared to the the above discussed 2N and 3N SRC cases:

$$E_m^{(3N-II)} = 2\sqrt{m^2 + p_m^2} - 2m - T_{A-1}. \tag{16}$$
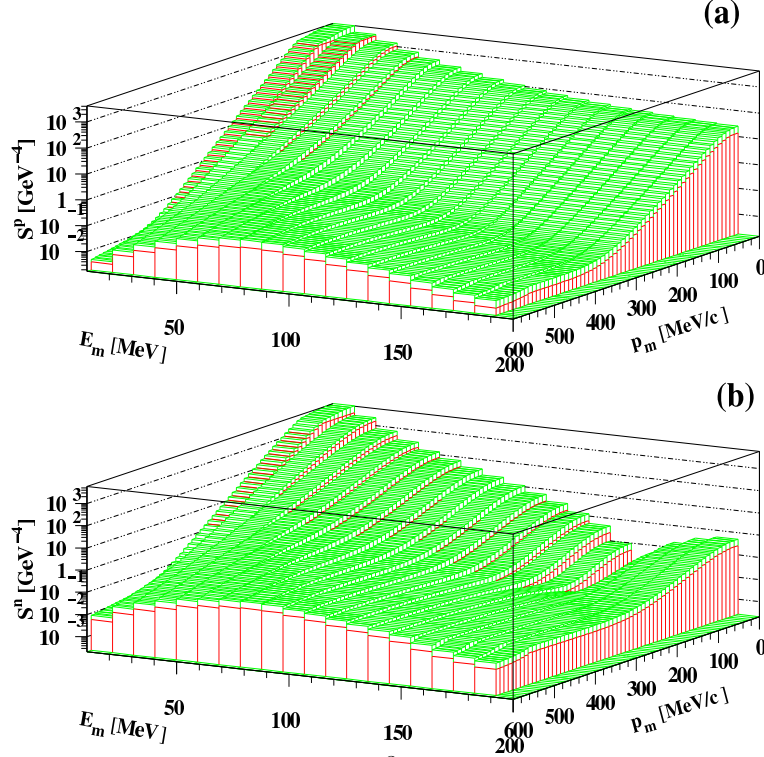
FIG. 3. (Color online) Spectral function for ${}^3He(e,e'N)X$ reaction for struck proton (a) and neutron (b) calculated within the PWIA and IA. The lines at the sides of the histograms shows the effects due to pair distortion.

A. Spectral Function

We start with the calculation of the spectral function as it is defined in Eq.(7). This quantity is relevant primarily for semi-exclusive $(e,e'N)$ reactions, in which only the scattered electron and knocked-out nucleon are registered. Figure 3 shows the spectral functions for the cases of knocked-out proton (a) and knocked-out neutron (b) calculated with the ${}^3He$ ground state wave function based on the Urbana-IX potential [11,14]. The hatched surface represents the PWIA prediction while dotted contours show the effect of pair distortion.

The correlation feature of Eq.(13) is reflected in the emergence of the broad peak in E_m distribution at $p_m \geq 300$ MeV/c, while the signature of 2N-II correlations is seen in the minimum of the E_m distribution at $p_m \approx 0$ for the case of knocked-out neutron with two recoil protons. This minimum reflects the fact that the relative momentum distribution in the pp pair has a node in the S-state at ≈ 420 MeV/c. These results are in agreement with previous analyses of spectral function [15].

The emergence of these correlations at $p_m \geq 300$ GeV/c are clearly seen in Fig.(4), in which solid and doted lines represent calculations within PWIA and IA approximations respectively. The positions of the peaks can be related to the dominance of type 2N-I SRCs in the high missing momentum part of the nuclear wave function [16,17] according to Eq.(13) (i.e. $E_m^{Peak} \approx E_m^{2N-I}$). The solid arrows in the figure correspond to the prediction of Eq.(13) corresponding to the scattering off a quasi-free and stationary two-nucleon correlation. This situation is reflected in the fact that, at large nucleon momenta p_m, the spectral function has similar functional dependence on p_m as the stationary two nucleon correlation [16]. It is worth noting that there were several experimental indications [18,19] of $E_m - p_m$ correlations according to Eq.(13). However, the lower values of Q^2 in these experiments did not allow direct discrimination of the short-range two-body forces from the long-range two-body currents corresponding to the meson-exchange contributions.
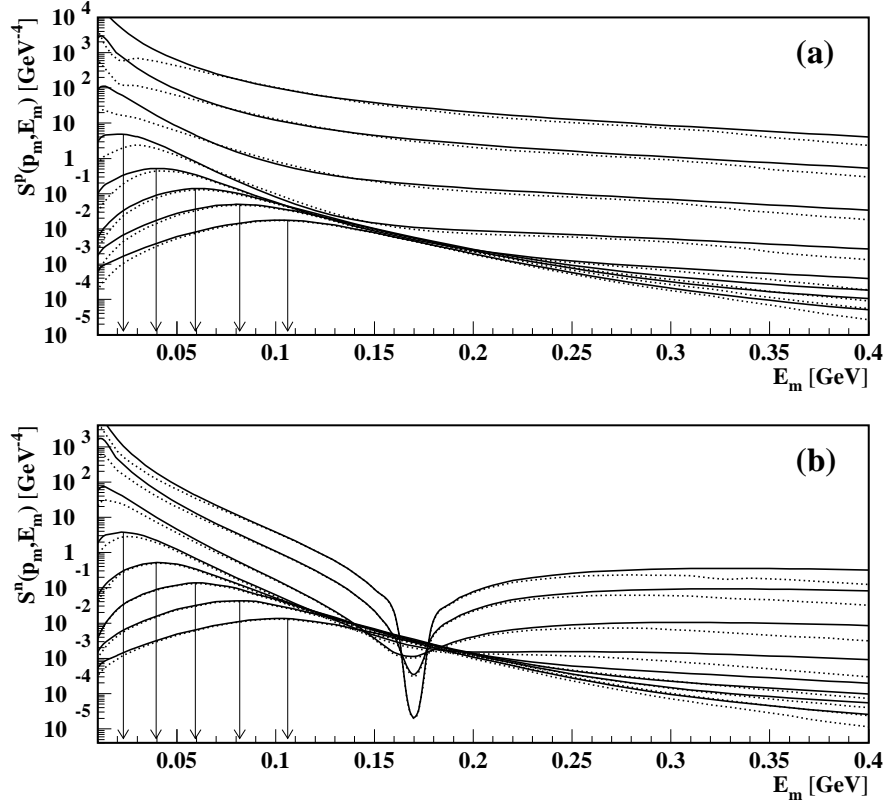
FIG. 4. Missing energy distribution of the spectral function for the removal of the proton (a) and neutron (b) at different values of missing momenta. Curves counted from the above at $E_m = 0$ correspond to the missing momenta 0 to 700 MeV/c with 100 MeV/c increments. Solid and dotted lines correspond to PWIA and IA predictions respectively. Arrows correspond to the prediction of Eq.(13)- scattering off a quasi-free stationary two-nucleon correlation.

The type 2N-II SRC can be identified clearly only for the spectral function involving two protons in the recoil kinematics, Fig.4(b). As Figs.3 and 4 demonstrate, no clear signatures are seen for 3N correlations. One expects type 3N-I correlations to dominate at the left corner of the E_m distribution starting at $p_m \geq 400 - 500$ MeV/c, while type 3N-II correlations dominate at the right (higher value) corner of the E_m distribution starting at

$p_m \gtrsim 400$ MeV/c. Fig.4 also demonstrates a strong dependence of pair-distortion effects on considered values of E_m and p_m.

1. Pair Distortion Effects

The pair distortion effects can be assessed quantitatively in Fig.5 which shows the missing momentum, p_m, distribution of the ratios of the spectral functions calculated within the PWIA and IA approximations for different values of E_m. These calculations demonstrate that the pair distortion strongly suppresses (by a factor of five) the spectral function at the kinematic region of small p_m and E_m. This reflects the fact that in this region two spectator nucleons have vanishing relative momentum at which the interaction cross section is very large. For the same reason, one observes significant pair distortion effects in the kinematics (see Eq.(15)) favorable for studies of type 3N-I correlations (high p_m part of the solid curve in Fig.(5)). Note that in this case pair distortion is larger for the pn recoil case than for the pp case.
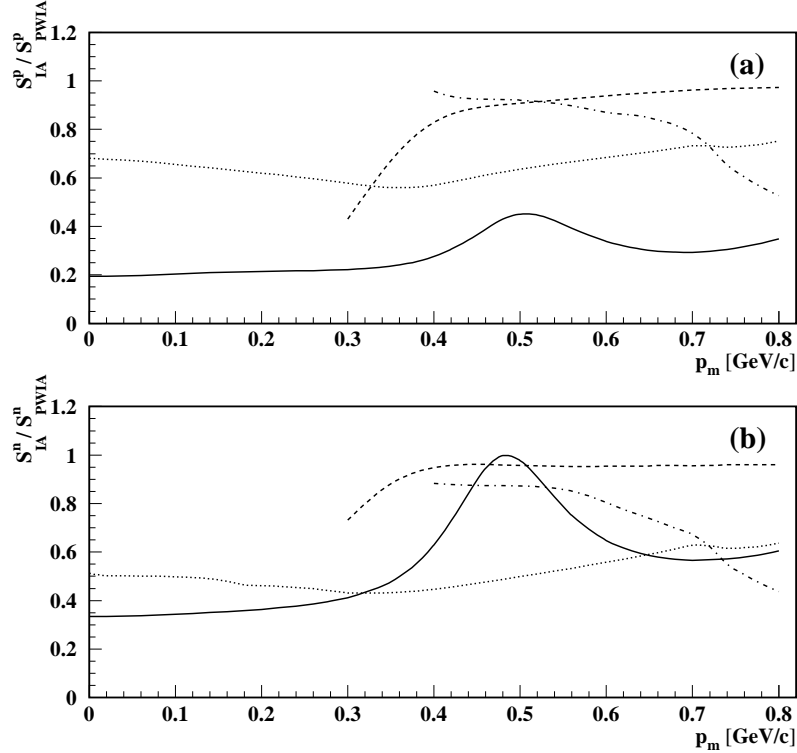
FIG. 5. Missing momentum dependence of the ratio of spectral function calculated within the IA and PWIA approximation. Solid lines correspond to $E_m = 0$. For the dashed lines, E_m is defined according to Eq.(13). For the dashed-dotted lines, E_m defined according to Eq.(16) and for dotted lines, $E_m = 350$ MeV.

Pair distortion is also large in the kinematics of very large $E_m > E_m^{2N-I,II}$ (dotted and dash doted lines in Fig.5) where one expects the dominance of type 3N-II correlations. The large pair distortion effects in the kinematics of 3N correlations can be understood qualitatively. The pair distortion effectively represents the three-nucleon correlation, in

which the initial short range NN correlation between knocked-out nucleon and one of the spectator nucleons is combined with the final state NN reinteraction between two recoil nucleons.

For type 2N-I correlations, Fig.5 (dashed lines) reveals modest pair distortion effects starting at $p_m \geq 400\text{MeV/c}$. At the same time, Fig.5 demonstrates more pair distortion for type 2N-II correlations. This result can also be understood qualitatively. For type 2N-I correlations, one of the recoil nucleons is initially in the SRC, while the second one is separated from the SRC with relatively small momentum. As a result, once one of the nucleons is instantaneously removed from the SRC, the two recoil nucleons in the final state will be spatially separated, thus reducing the probability for their interaction.
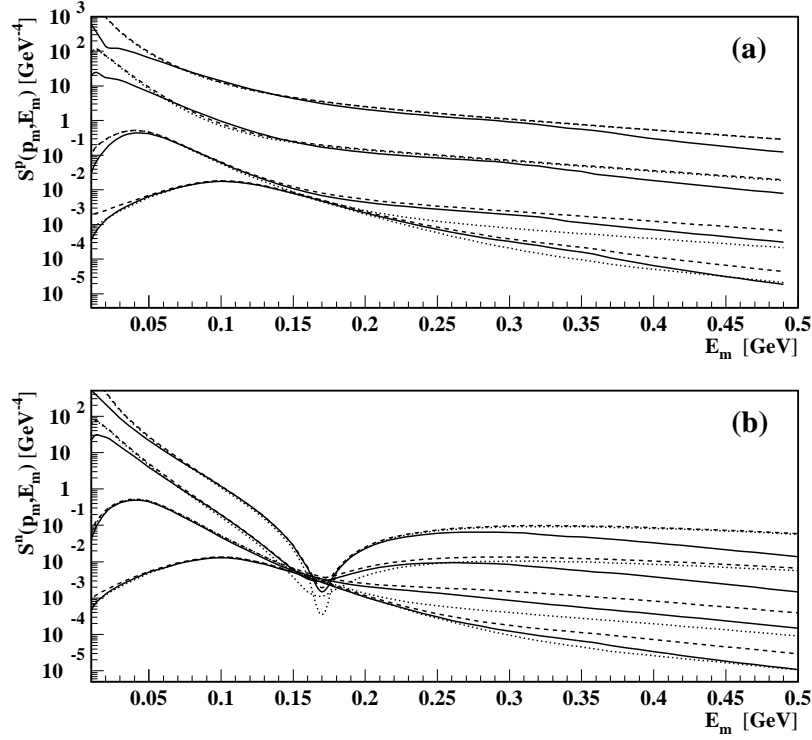
FIG. 6. Missing momentum dependence of the spectral function at different values of missing momenta. The curves counted from the upper left to the lower left of the figures correspond to the missing momenta 100, 200, 400 and 700 MeV/c. Dotted lines – PWIA prediction with only NN potential considered, dashed line – PWIA with additional 3N forces included, solid line – IA with the same 3N forces included.

The situation is different for type 2N-II correlations in which two recoil nucleons are in the SRC and are spatially close to each other. This will result in much larger pair distortion effects than for type 2N-I correlations. The observed feature is consistent with the qualitative arguments of Ref. [16,6] that to break the SRC and release a spectator from it with minimal distortion it is preferable to knock-out a nucleon directly from the SRC.

The next question we address is whether the spectral function can provide an effective framework for studies of the implication of three nucleon forces (3NFs) in the ground state wave function of ^3He. Qualitatively, one expects that the onset of 3NFs to arise in the kinematics dominated by three-nucleon correlations. This expectation is confirmed in Fig.6

where the main 3NF effects are seen at $E_m = |\epsilon_A|$ and $E_m > E_m^{2N-I,II}$. Here we consider the difference in the predictions of the spectral functions calculated based on the ^3He wave functions which are calculated with and without explicit inclusion of 3NFs (see e.g. [11]). Predictions are made within PWIA are denoted by dotted and dashed lines in Fig.6.

However, as it was discussed above, in the same region of E_m and p_m we predict sizable effects due to pair distortion, which effectively imitates a three-nucleon correlation. As Fig.6 demonstrates pair distortion (solid lines) will considerably diminish signatures related to 3NF effects in the spectral function.
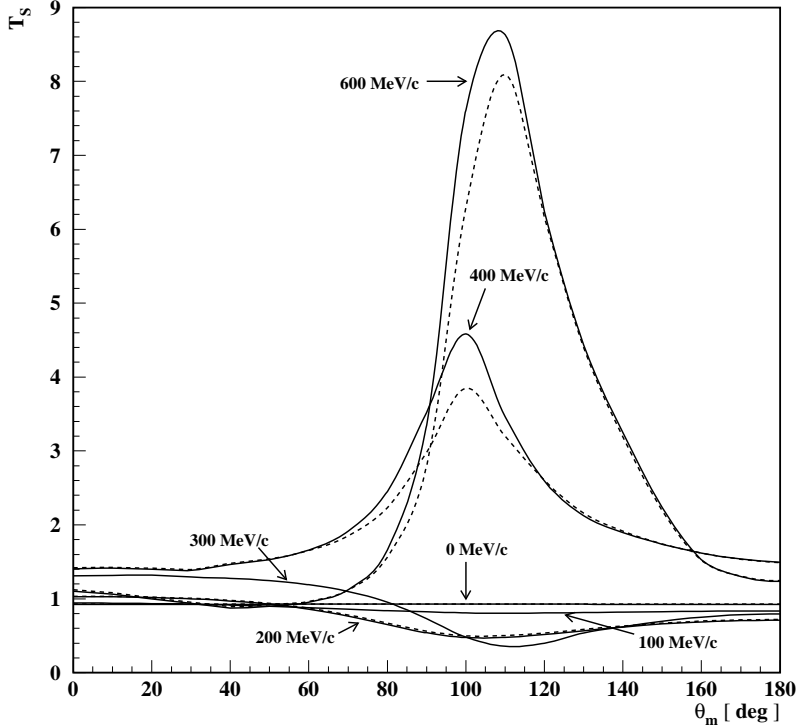
FIG. 7. Angular dependence of transparency T as defined in Eq.(17) for the reaction with struck proton at different values of missing momenta. The missing energy here is defined according to type 2N-I correlation condition of Eq.(13). Solid line – only single rescattering amplitude is included in FSI, dashed line – both single and double rescattering amplitudes are included in FSI.

2. Final state interaction (FSI) effects

The inclusion of the FSI of the knocked-out nucleon with spectator nucleons removes the isotropy of spectral function with respect to the direction of the virtual photon, $\mathbf{q}$. To asses the FSI effects quantitatively, we analyze the ratio, T_S, defined as follows:

$$T_S = \frac{S_{DWIA}^N(Q^2, q, E_m, p_m)}{S_{IA}^N(E_m, p_m)}, \tag{17}$$

where subscripts $DWIA$ and IA denote the spectral functions calculated with and without FSI effects. Here $T_S \approx 1$ corresponds to the small effects of the FSI, while $T > 1$ or $T < 1$ will indicate the dominance of the absorption or the rescattering effects due to the FSI.

13

Based on the analysis of the analytic properties of rescattering amplitudes in GEA [2], it is possible to identify the kinematic regions in which one can isolate the FSI or the SRC as the dominant term in the scattering amplitude.

Similar to the reaction of exclusive electro-disintegration of the deuteron [20], one expects the FSI to dominate in nearly transverse kinematics in which $\alpha_m = 1$ and $p_m \geq 100$ MeV/c. Here, α_m in the IA describes the momentum fraction of the nucleus carried out by a nucleon "1" in the infinite momentum frame of the nucleus. It is defined as follows:

$$\alpha_m = \frac{p_{m-}}{p_{A-}} \approx \frac{p_{f-} - q_-}{m} \mid_{Lab\ Frame}, \tag{18}$$

where the "minus" components of momenta are defined by $k_- = k_0 - k_z$.

Fig.7 represents the θ_m (α_m) dependence of T_S at different values of p_m calculated at $Q^2 = 4$ GeV^2. The missing energy in these calculations is chosen for the type 2N-I correlation (Eq.(13)). The figure demonstrates the presence of significant FSI effects in the near-transverse kinematics, $\alpha_m \approx 1$, with the effects diminishing at parallel ($\theta_m = 0^0$) and anti-parallel ($\theta_m = 180^0$) kinematics [3].

The missing energy E_m, gives us an additional degrees of freedom to "manipulate" the relative strength of the FSI and SRC effects in the different kinematics of electro-disintegration. This is especially important for isolating SRC structures in the spectral function as it is measured in $A(e, e'N)X$ reaction. In the beginning of Sec.IV, we identified several kinematic regions in which the strength of the spectral function is largely determined by SRCs. In all these cases, the initial momenta of at least two nucleons in the nucleus exceeds $300 - 400$ MeV/c. The final state reinteraction of the knocked-out nucleon with the spectator nucleons can largely destroy this picture. For example, as can be seen from Eqs.(21) and (27) in Ref. [1], due to the integration in the rescattering loops, it is impossible to ensure the appearance of large values of internal momenta in the ground state wave function of the nucleus in a straightforward way. Thus, the condition $p_m \geq 300$ MeV/c or $E_m \gtrsim 100$ MeV may not ensure the dominance of the high-momentum component in the ground state wave function of the nucleus. This situation may significantly affect the identification of type 2N and 3N correlations.

The problem of suppression of the FSI in probing the SRC in the $A(e, e'N)X$ reaction was addressed within the GEA in Ref. [2]. It was observed that a trivial condition, $p_m \geq k_F$, is not sufficient to probe the SRC component of the ground state nuclear wave function. One needs to impose the following additional condition on the effective longitudinal momentum, p_Z, entering the single rescattering amplitude,

$$p_Z \equiv p_{mz} + \frac{q_0}{q}(E_m + \frac{p_m^2}{4m}) > k_F. \tag{19}$$

With this, one will ensure that rescatterings happen within the SRC. Note that "p_Z"s in Eq.(19) correspond to the pole values of fast nucleon propagators in the rescattering amplitude (see e.g. Eq.(21) in Ref. [1]).

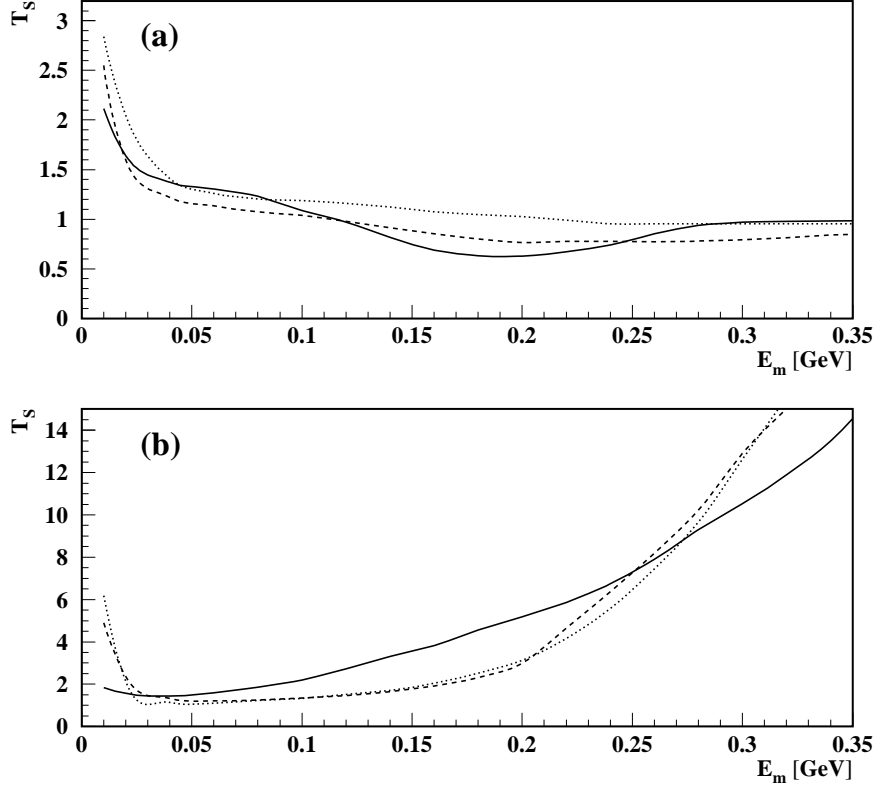[3]Everywhere in the text parallel/anti-parallel kinematics correspond to $\theta_m = 0^0/180^0$

FIG. 8. Missing energy dependence of transparencies for the knocked-out proton reaction at parallel, $\theta_m = 0^0$, (a) and anti-parallel, $\theta_m = 180^0$, (b) kinematics. The solid, dashed and dotted curves corresponds to the calculation with missing momenta equal to 400, 500 and 600 MeV/c respectively.

In Fig.8, we consider the E_m (p_Z) dependence of T_S for parallel (a) and anti-parallel (b) kinematics for values of p_m equal to 400, 500 and 600 MeV/c. In Fig.8(a), the center of mass momentum of the two recoil nucleons is in the direction backward to $\mathbf{q}$, while in Fig.8(b), the recoil system is produced in the forward direction. One can see from this figure that the FSI indeed decreases with increase of $|p_Z|$. This indicates that the FSI is increasingly confined within the SRC. An interesting feature of these results is that while the FSI contribution keeps decreasing with increase of $|p_Z|$ in the kinematic region relevant for type 2N-I and 3N-II correlations, it grows sharply in the region associated with the type 3N-I correlations. Both trends can be understood qualitatively. When $|p_Z| \leq k_F$, one has dominant contributions from the FSI involving uncorrelated nucleons which have a larger probability amplitude in the ground state wave function of ^3He. Once $|p_Z| > k_F$, the FSI takes place predominantly within the 2N correlation. In the latter case, for type 2N-I SRC, the third nucleon has a small momentum and is spatially separated from the NN SRC. Thus, it does not contribute substantially to the FSI.
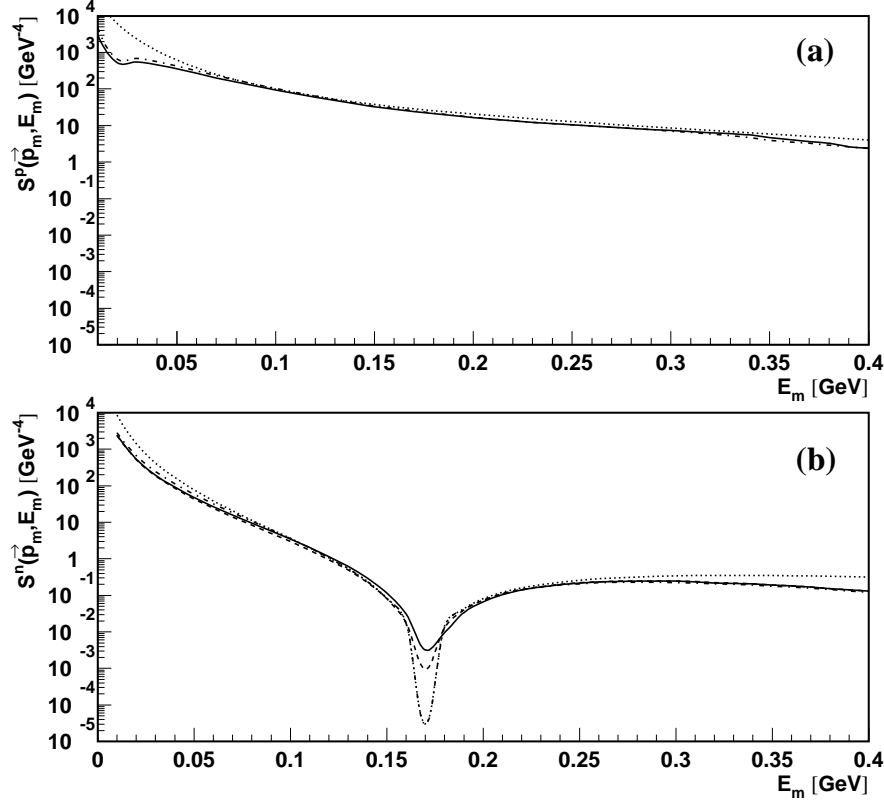
FIG. 9. Missing energy dependence of the spectral function for the type 2N-II correlation condition at missing momentum $p_m = 0$. Dotted, dashed-dotted, dashed and solid lines correspond to PWIA, IA, IA+FSI1 and full (IA+FSI) calculations respectively.

For type 3N-I correlations both spectator nucleons contribute to the FSI since they are both correlated with the knocked-out nucleon. This results in larger FSI effects as compared to the IA contribution. These calculations indicate that (except for the case of type 3N-II SRC in the parallel kinematics) the FSI generally dominates in the kinematics where one expects an enhanced contribution from 3N SRCs in the wave function of ^3He.

For type 2N-II correlations, the FSI takes place between the knocked-out nucleon, which is initially almost at rest and spatially separated from the 2N SRC (see Fig.1(b)). As a result, one expects a diminished FSI contribution in whole range of E_m. Such behavior can be seen in Fig.9 for the calculated E_m dependence of the spectral function at $p_m = 0$. This calculation shows that the type 2N-II SRC for the knocked-out neutron reaction attains the characteristic minimum in E_m distribution although smeared out strongly due to rescatterings.

In Fig.10 we summarize the predictions for the E_m dependence for the spectral function at different values of missing momenta p_m calculated for parallel (a) and anti-parallel (b) kinematics. These calculations demonstrate that the observed $E_m - p_m$ correlation within the IA for type 2N-I SRC generally survives the FSI for both parallel and anti-parallel kinematics. For 3N correlations, type 3N-II SRC survives FSI for parallel kinematics while type 3N-I SRC is strongly affected by FSI.

16

Summarizing our consideration of the spectral function we can conclude that the $A(e, e'N)X$ reaction is best suited for studies of 2N correlations only. Type 2N-I SRC survives both pair distortion and the FSI while type 2N-II attains its specific feature for neutron-knock out reactions at $p_m \leq 100$ MeV/c [4].
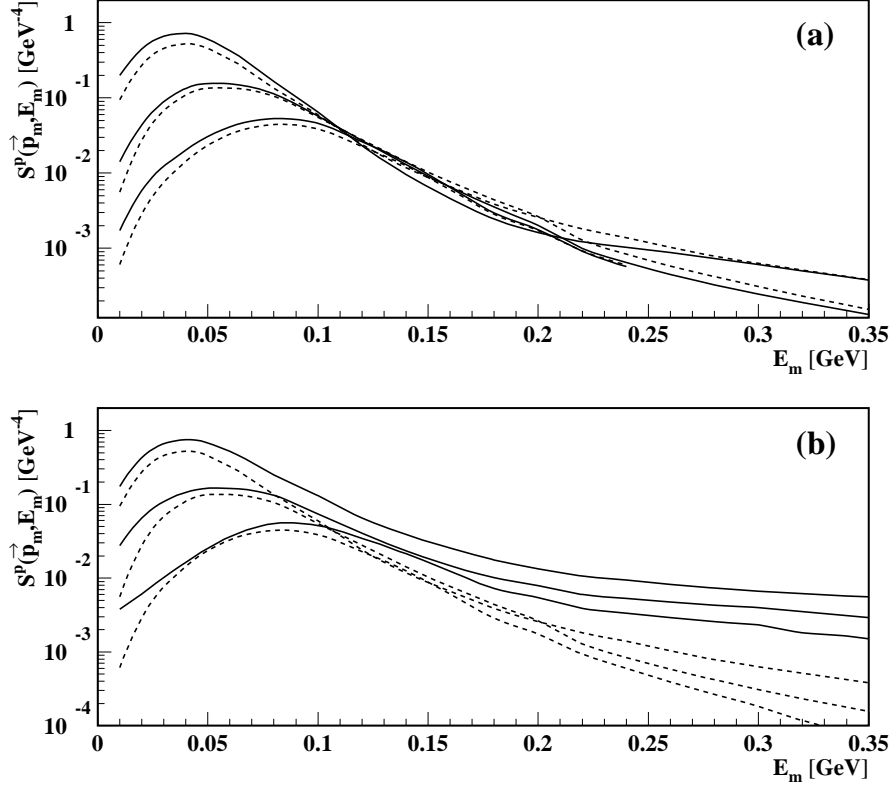

FIG. 10. Missing energy dependence of the spectral function for the knocked-out proton reaction in parallel (a) and anti-parallel (b) kinematics at different values of missing momenta. The upper, middle and lower curves at the left corner of the figure correspond to the missing momenta 400, 500 and 600 MeV/c respectively. Dashed line – IA prediction, solid line IA+FSI prediction.

Our calculations show that, in general, 3N correlations are strongly affected by pair distortion and FSI effects. Pair distortion, having a qualitative features of 3N correlation, strongly affects both types of 3N correlations, while the FSI contributes strongly in type 3N-I SRC and has a diminished impact on type 3N-II SRCs only at parallel kinematics.

Finally, for near transverse kinematics starting at $p_m \geq 400$ MeV/c, the $A(e, e'N)X$ reactions represent an ideal tool for studying the structure of FSIs. This feature becomes especially valuable for large $Q^2 > 4$ GeV^2 for studies of color coherence phenomena for which we expect a decrease of T_S with an increase of Q^2 as opposed to the Q^2 independence of T_S in the GEA.

---

[4]As a note of caution, we point out that the minimum in the E_m distribution is very narrow. Hence its experimental observation will require resolution in E_m on the order of a few MeV.
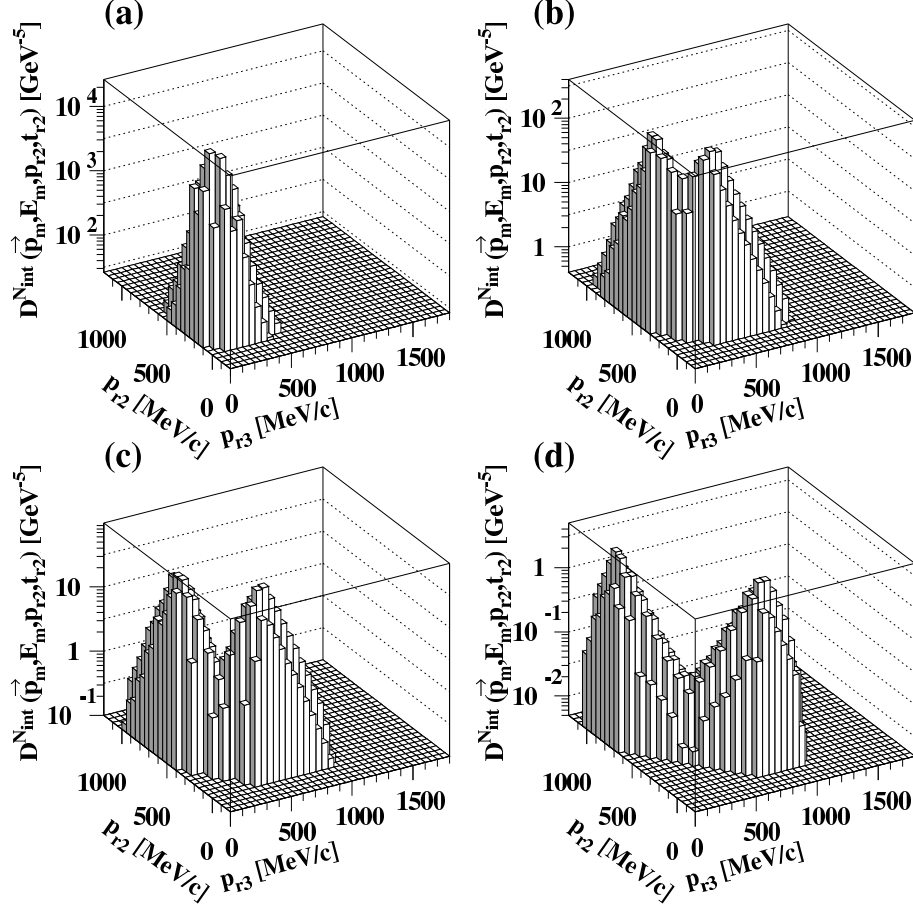
FIG. 11. Dependence of the decay function on the momenta of the two recoil protons p_{r2} and p_{r3} at different cuts of missing momentum of the knocked-out neutron. (a)$p_m > 150$ MeV/c, (b)$p_m > 300$ MeV/c, (c)$p_m > 400$ MeV/c and (d)$p_m > 700$ MeV/c.

B. Decay Function

The decay function is practically an unexplored quantity and the experiments that will allow us to extract it from the exclusive cross section data are only emerging [21]. Our main motivation in these numerical analyses is to highlight those significant features of the decay function that are related to the short-range structure of the ground state nuclear wave function as well was to the structure of reinteractions between the nucleons in the final state of the reaction.

We will consider the partially integrated decay function, which will allow us to remove the δ-function in Eqs.(9) and (10). Namely, we consider,

$$D_{int}^N(\mathbf{p_m}, E_m, p_{r2}, t_{r2}) = \int D^N(\mathbf{p_m}, E_m, \mathbf{p_{r2}}, t_{r2}) p_{r2}^2 d\Omega_{r2}, \qquad (20)$$

where $D^N(\mathbf{p_m}, E_m, \mathbf{p_{r2}})$ is defined in Eqs.(9) or (10). This integration takes into account the fact that one of the components of $\mathbf{p_m}$ or $\mathbf{p_{r2}}$ is not independent and is fixed from the energy conservation condition for the quasi-elastic disintegration of ^3He. Therefore, D_{int} represents a quantity which could be extracted directly from a $^3He(e, e'NN)N$ experiment. Furthermore, we will refer to D_{int} as a decay function.
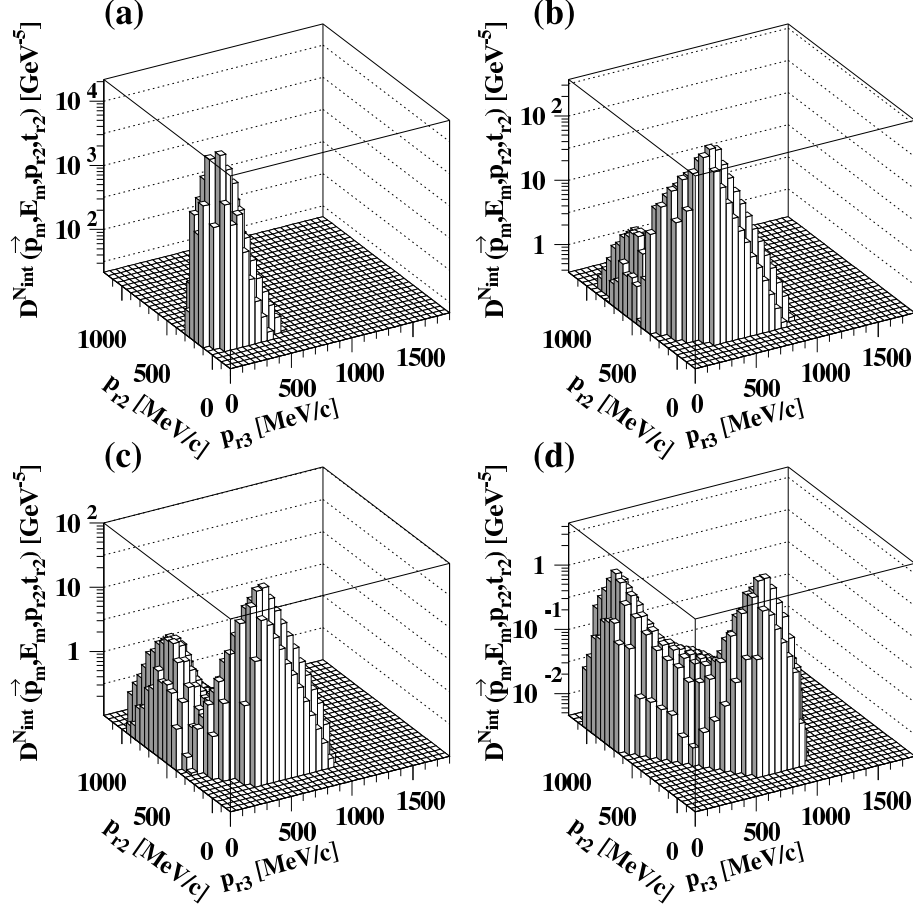
18

FIG. 12. The same as in Fig.11 for proton and neutron recoil with momenta p_{r2} and p_{r3} respectively.

We start by analyzing the decay function in the PWIA, focusing on those features that are related to SRC signatures of the ground state wave function which are described in Figs.1 and 2. As we observed in the previous section, type 2N-I SRCs exhibited measurable (though broad) correlation between E_m and p_m (starting at $p_m \geq 300$ MeV/c), with the peak of the E_m distribution defined by Eq.(13). These correlations could be understood qualitatively as a result of strong short range interactions between the struck nucleon (with momentum p_m) and one of the recoil nucleons in the nucleus with the third nucleon having a relatively small momentum in the mean field of the 2N SRC pair. To check this picture, we calculate the decay function distribution as a function of p_{r2} and p_{r3} imposing different cuts on the missing momentum, p_m.

Figs.11 and 12 present the results of the calculation of the decay function of the reactions corresponding to the knock-out of the neutron and proton respectively. The (a), (b), (c) and (d) parts correspond to the p_m cuts at $p_m >$ 150, 300, 400 and 700 MeV/c respectively. The calculations clearly show emerging type 2N-I correlations between the knocked-out nucleon and one of the spectator nucleons with an increase of p_m. These correlations are dominating the landscape of the (p_{r2}, p_{r3}) distribution once $p_m \geq 300 MeV/c$. Fig.12 shows also that the pn SRCs are significantly larger than the pp correlations. Thus, measuring the decay function will allow a direct check of the relative strength of pp and pn correlations. We conclude, from the discussions of Figs.11 and 12, that the decay function is strikingly more

19

sensitive to the SRC than the $E_m - p_m$ correlation observed in the spectral function.
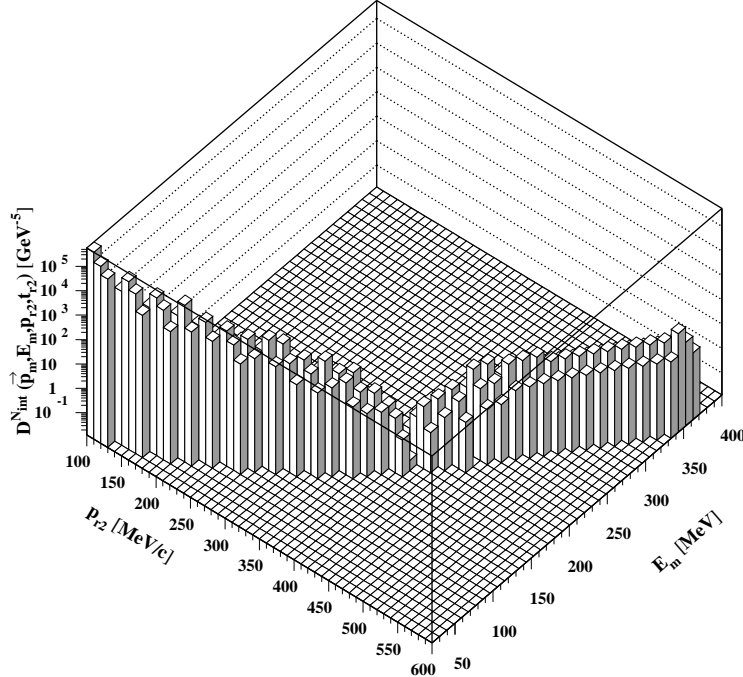

FIG. 13. The (E_m, p_{r2}) distribution of the decay function for the neutron knockout reaction. The missing momentum is restricted to $p_m < 50$ MeV/c.

Next we analyze the features of the decay function related to the type 2N-II correlations. From the consideration of the spectral function in the previous section, we learned that reactions corresponding to the knock-out of the neutron are best suited for studies of type 2N-II correlations since, at small $p_m < 100$ MeV/c and large E_m, the spectral function exhibits a minimum associated with the node in the relative momentum distribution of the recoil pp pair in the S-state. In Fig.13 we show the (E_m, p_{r2}) distribution of the decay function which demonstrates strong correlations between the minimum in the E_m distribution and the value of recoil nucleon momenta at small p_m (< 50 MeV/c in the calculation).

Turning now to the three nucleon correlations, we observe that for both types of 3N SRCs (Fig.2) the two recoil nucleons have comparable momenta. This situation corresponds kinematically to the area around the saddle in Figs.11 and 12. One can check whether the expectation that type 3N-I and 3N-II correlations will dominate in the dynamics of three nucleon correlations is justified. For this we observe that the configurations of Fig.2 are characterized by a distinctive angular relations between the two recoil nucleons: for type 3N-I SRC two recoil nucleons will be produced at small relative angle (almost parallel) while for type 3N-II SRC the relative angle of the recoil nucleon momenta is $\approx 120^o$. In Fig.14 we analyze the dependence of the decay function on the relative angle between the recoil nucleons, θ_{23}, and the missing energy, E_m, for different values of missing momentum, p_m.

Fig.14(c) and (d) clearly show an emergence of peaks at small E_m and θ_{23} (type 3N-I SRCs) and at large E_m and $\theta_{23} \approx 120^0$ (type 3N-II SRCs). The appearance of the peaks is more clearly seen in Fig.15 where Fig.14 (d) is demonstrated from different viewpoints. Fig.15 shows also the peak at $\theta_{23} \approx 180^0$ and at moderate values of E_m which corresponds to the type 2N-I correlation in which only one of the recoil nucleons is correlated with the

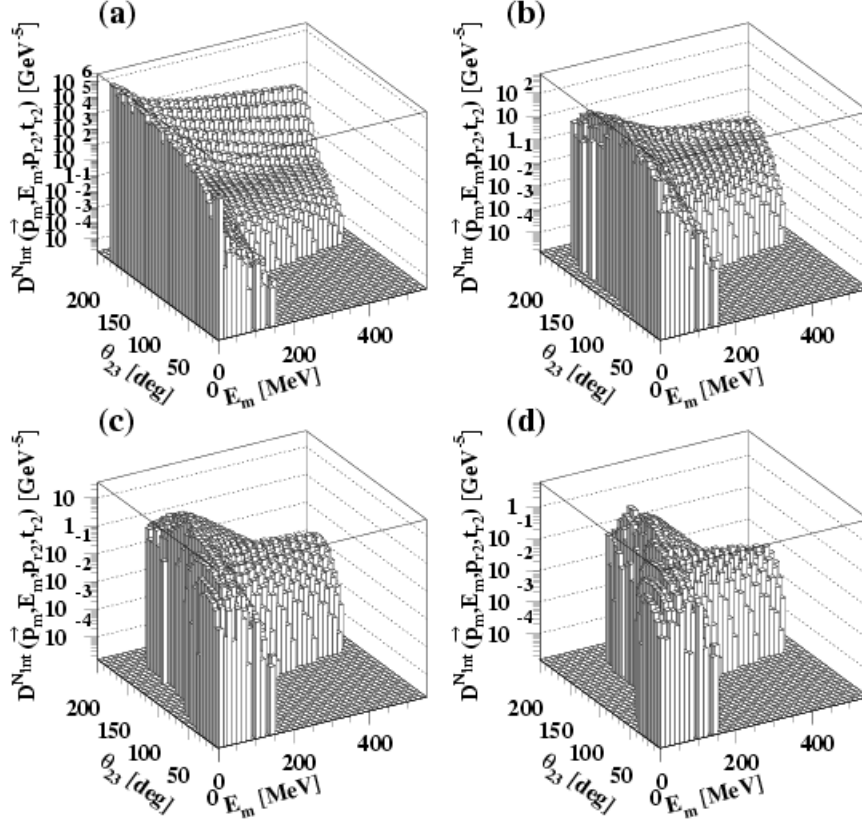knocked-out nucleon and is produced in the direction opposite to the direction of $\mathbf{p_m}$.

FIG. 14. The dependence of the decay function of the reaction $^3He(e,e'pp)n$ on the relative angle between the recoil pn nucleons, θ_{23}, and the missing energy, E_m, for different cuts of missing momentum, p_m. (a) – no cuts on p_m, (b) – $p_m > 300$ MeV/c, (c) – $p_m > 500$ MeV/c, (d) – $p_m > 700$ MeV/c.

Moving to a more quantitative discussion of correlation properties of the decay function, in the following subsections we study the following question: To what degree do the detected properties of the recoil nucleon in coincidence with the knocked-out nucleon reflect the properties of preexisting short range configurations in the ground state nuclear wave function?

1. Pair Distortion Effects

In Fig.16 we discuss the effects of the reinteraction between recoil nucleons (pair distortion) in the p_{r2}-momentum distribution of the decay function for all four types of correlations[5]. In Fig.16(a) one observes a significant difference in the yields of the recoil

---

[5]Herewith, we will label calculations by (N_f, N_{r2}), in which N_f and N_{r2} describe the type of the knocked-out and recoil nucleons with momenta $\mathbf{p_f} = \mathbf{p_m} + \mathbf{q}$ and $\mathbf{p_{r2}}$ respectively.

proton or neutron for a reaction in which one of the protons is knocked out from the type 2N-I correlations. Fig.16(b) shows the momentum distribution of the recoil proton when proton (labeled "pp" in the figure) or neutron (labeled "np") is knocked-out in the kinematics of type 2N-II correlations.
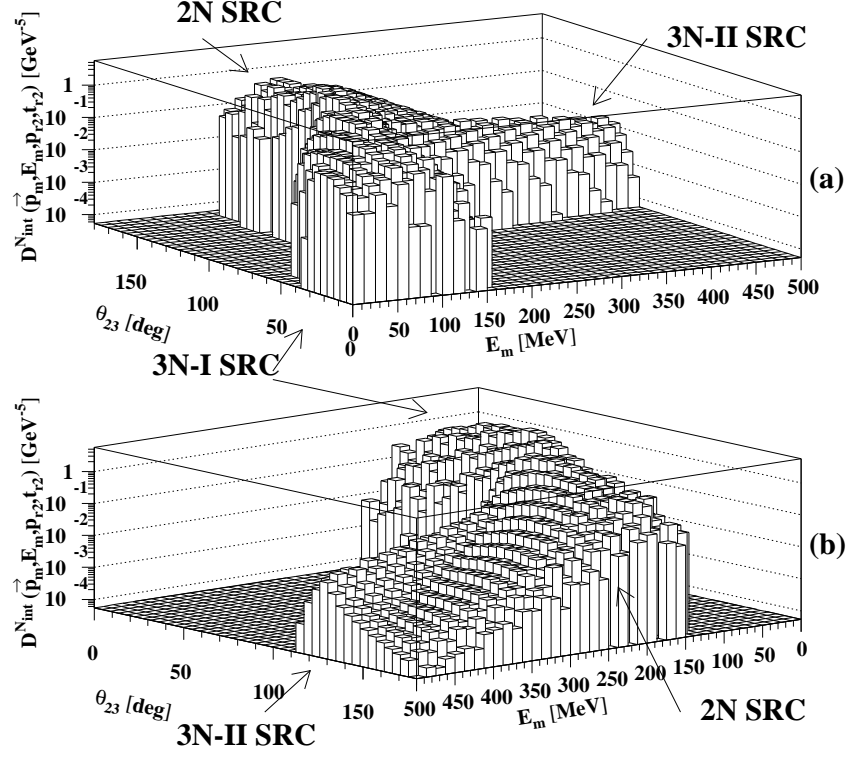

FIG. 15. Reproduction of Fig.14d from different viewpoints to emphasize the signatures of type 3N-I (a) and type 3N-II (b) correlations.

This figure demonstrates significant pair distortion effects as compared to the type 2N-I correlations. Figs.16(c) and (d) demonstrate the momentum distributions from type 3N-I and II SRC's respectively. As in the case of the spectral function, one observes that, in general, the pair distortion interferes significantly with the three nucleon correlations. It is worth noting, however, that, due to the depleted interaction strength in the pp channel at relative momenta ~ 400 MeV/c, pair distortion effects are suppressed in type 3N-II correlations for the neutron knock-out reaction in a recoil momentum range of $300 - 550$ MeV/c (see Fig.16(d)). We will discuss in Sec.IV B 4 how this observation could be used to explore the type 3N-II kinematics for investigation of three nucleon forces in ^3He.

Also, Fig.16 reveals an additional feature that allows us to discriminate between 2N and 3N SRC signals. This feature is the relative abundance of pp and pn pairs in different correlations. For 2N correlations one observes significantly smaller yield associated with pp correlations as compared to pn correlations while for 3N correlations these yields are comparable.
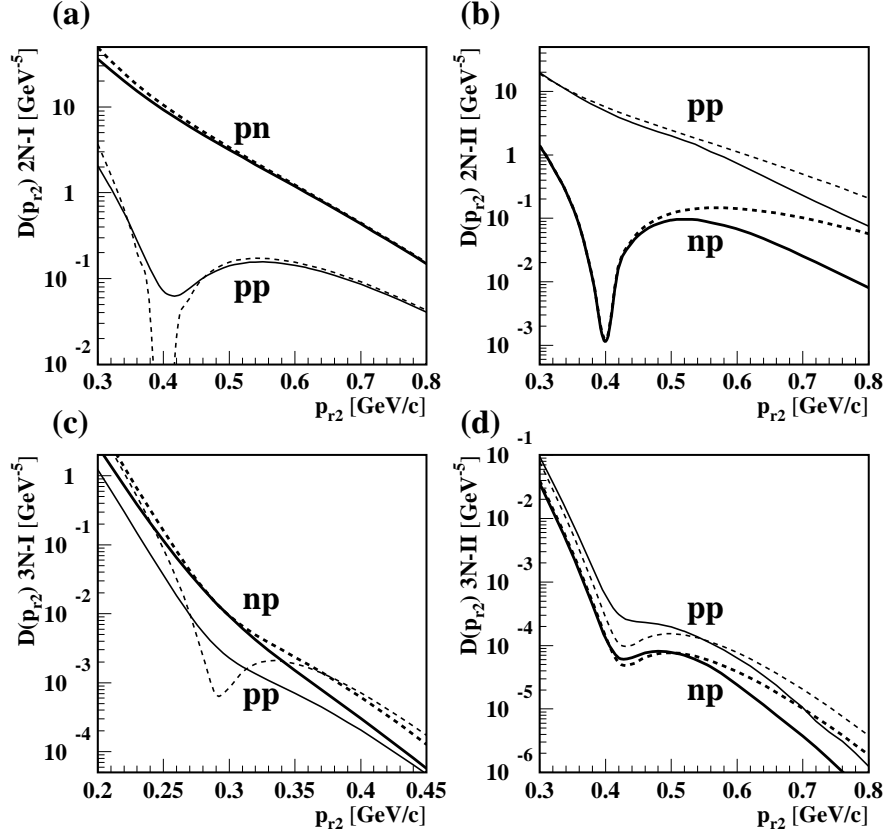
FIG. 16. Dependence of the decay function on the momentum of the registered recoil nucleon, p_{r2}, in $^3He(e, e'N_fN_{r2})N_{r3}$ reactions.(a), (b), (c) and (d) correspond to types 2N-I, 2N-II, 3N-I and 3N-II kinematics respectively. Dashed lines – PWIA prediction, solid lines - IA predictions. Two pairs of curves in each figure correspond to different compositions of detected nucleons (N_f, N_{r2}).

2. Final State Interaction

The inclusion of the final state interaction of the knocked-out nucleon with residual nucleons removes the isotropy of the decay function with respect to the momentum vector of the virtual photon, **q**. Staying in the framework of consideration of type 2N and 3N correlations, we investigate FSI effects in angular and momentum dependences of the decay function for each type of correlation. As in Sec.IV A 2, we consider the kinematics with fixed $Q^2 = 4$ GeV^2.

A. Type 2N-I Correlations:

For the type 2N-I correlations, we consider first the dependence of the decay function on the production angle of recoil nucleon N_{r2} with respect to the direction of the virtual momentum **q**. Fig.17 shows these dependences for different values of recoil nucleon (neutron (a) and proton (b)) momentum p_{r2} for the reaction with knocked-out proton. Calculations clearly show the transition of FSI from the screening regime at momenta $p_{r2} \leq 300$ MeV/c to the

double scattering regime at $p_{r_2} \geq 400$ MeV/c. This picture is clearly reminiscent the double scattering signatures of the deuteron electro-disintegration [20,2,3].
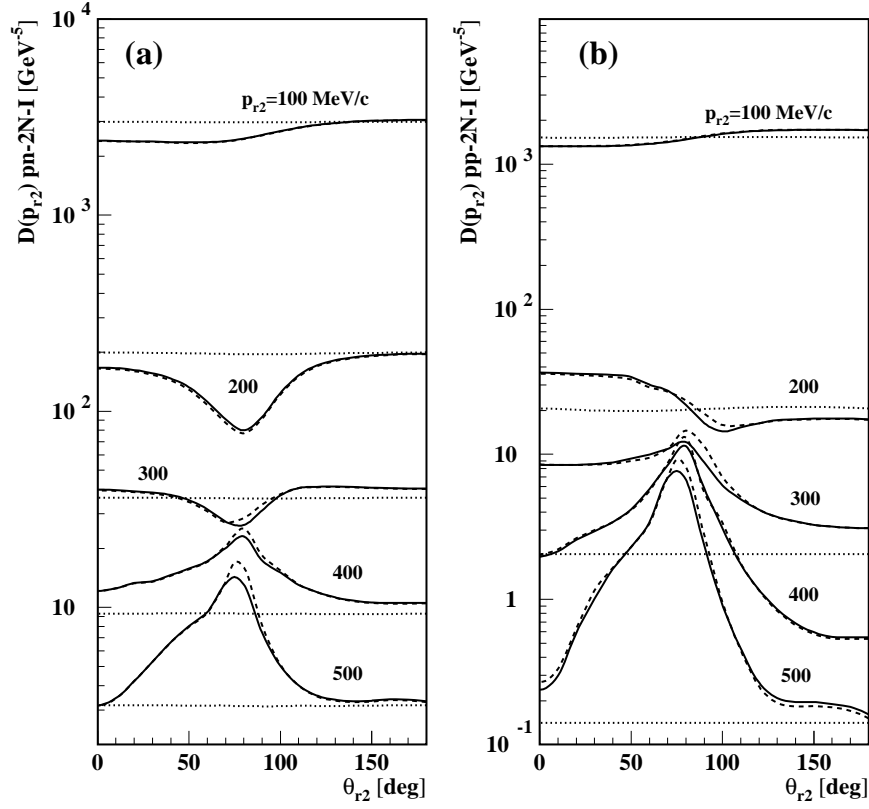

FIG. 17. Dependence of the decay function on the angle of the detected recoil nucleon, θ_{r2}, with respect to **q** for different and fixed values of p_{r2}. The decay function is calculated for type 2N-I SRC kinematics. (a) $-(N_f, N_{r2}) \equiv (p, n)$, (b)$- (N_f, N_{r2}) \equiv (p, p)$. Dotted lines - IA, dashed lines - IA+FSI1 (Single Rescattering only), solid line - IA+FSI. Note that for figure (b) the IA contribution at $p_{r2} = 400$ MeV/c is not shown since it is negligible due to the node in the pp momentum distribution.

Calculations also predict very different angular dependences for neutron (a) and proton (b) production in recoil kinematics. It is easy to check that the maximal FSI effects are predicted at $\alpha_{r2} = \frac{E_{r2} - p_{r2}^z}{m} = 1$ which is analogous to the maximums of the FSI for the spectral functions at $\alpha_m = 1$ observed in Sec.IV A 2. Fig.17 shows also that our best chances to extract genuine information about type 2N-I SRC, is to concentrate on anti-parallel ($\theta_{r2} = 0^0$) and parallel ($\theta_{r2} = 180^0$) kinematics. It is worth noting that the range of θ_{r2} where FSI, are small is broader for the $\theta_{r2} = 180^0$ case.

Fig.18 represents the p_{r2} momentum dependences of the decay function for $\theta_{r2} = 180^0$ and $\theta_{r2} = 0^0$ (marked curves) kinematics. Calculations predict qualitatively different momentum distributions for correlated pn (a) and pp (b) pairs. While for pn at both $\theta_{r2} = 180^0$ and $\theta_{r2} = 0^0$ one observes qualitatively similar momentum distributions, for pp pairs they are significantly different. This difference can be understood from Eq.(19), which defines the effective longitudinal component of missing momentum entering in the rescattering am-

24

plitude. For type 2N-I kinematics it can be written as $p_Z = -p_{r2}cos(\theta_{r2}) + \frac{q_0}{q}(E_m + \frac{p_{r2}^2}{4m})$. At $\theta_{r2} = 180^0$ $(\theta_{r2} = 0^0)$, $p_Z > (<)p_{r2}^z$ and the FSI term is defined by the effective momentum which is larger (smaller) than measured momentum, p_{r2}. As a result, the FSI is suppressed at $\theta_{r2} = 180^0$ (backward) kinematics as compared to the $\theta_{r2} = 0^0$ (forward) kinematics. For the pp pair this difference is very dramatic due to the node in the relative momentum distribution of the pp pair.
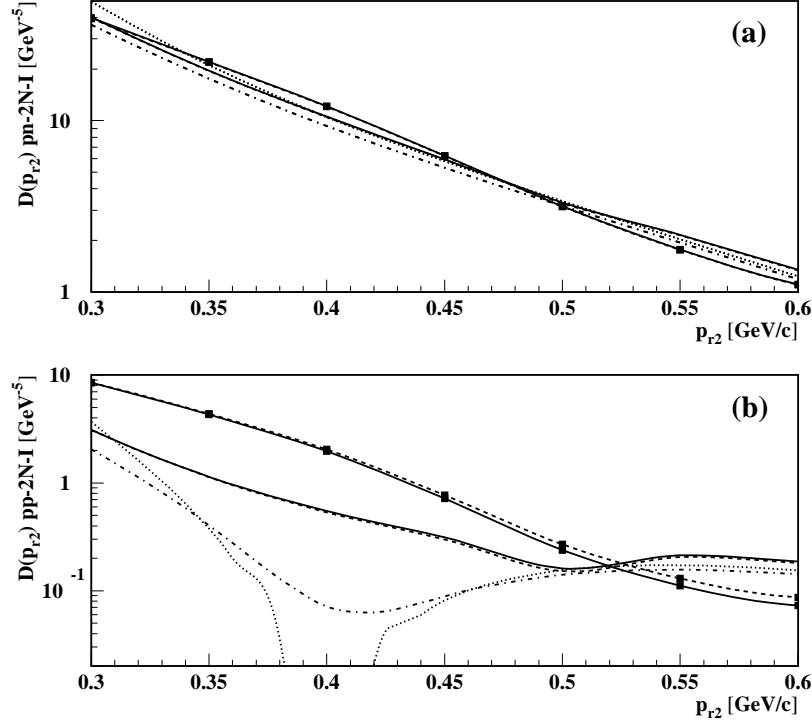
FIG. 18. Dependence of the decay function on the momentum of the recoil nucleon, p_{r2} calculated for the kinematics of type 2N-I correlations (a) – $(N_f, N_{r2}) \equiv (p, n)$ and (b)– $(N_f, N_{r2}) \equiv (p, p)$. Doted lines - IA prediction, dashed and solid lines for IA+FSI1 and IA+FSI predictions respectively for parallel $\theta_m = 0^0$ kinematics. Curves with square labels correspond to IA+FSI1 and IA+FSI predictions for anti-parallel $\theta_m = 180^0$ kinematics.

It is worth noting that no significant triple scattering (double rescattering) contribution is observed in Figs.17 and 18. This serves as an additional indication that in type 2N-I kinematics the reaction is defined predominantly by two-body interactions, thus representing a nearly ideal framework for studies of the 2N processes both in terms of the short range correlations and single rescattering processes.

B. Type 2N-II Correlations:

To isolate type 2N-II correlations we identify kinematics similar to one presented in Fig.16(b), in which missing momentum is fixed to $p_m = 100$ MeV/c in $\mathbf{q}$ direction. In Fig.19 we consider the θ_{r2} dependence of the decay function for both pp (a) and pn (b) recoil pairs. Since, in these kinematics, the knocked-out nucleon is on average at a larger distance from the recoil 2N pair, one expects the lesser FSI effects due to rescattering of the knocked-out

nucleon off the recoil nucleons. Calculations presented in Fig.19 confirm this expectation. The same pattern can be seen in the momentum distribution plot in Fig.20 which shows that the FSI is diminished practically for the whole region of recoil nucleon momenta, p_{r2}, of interest.
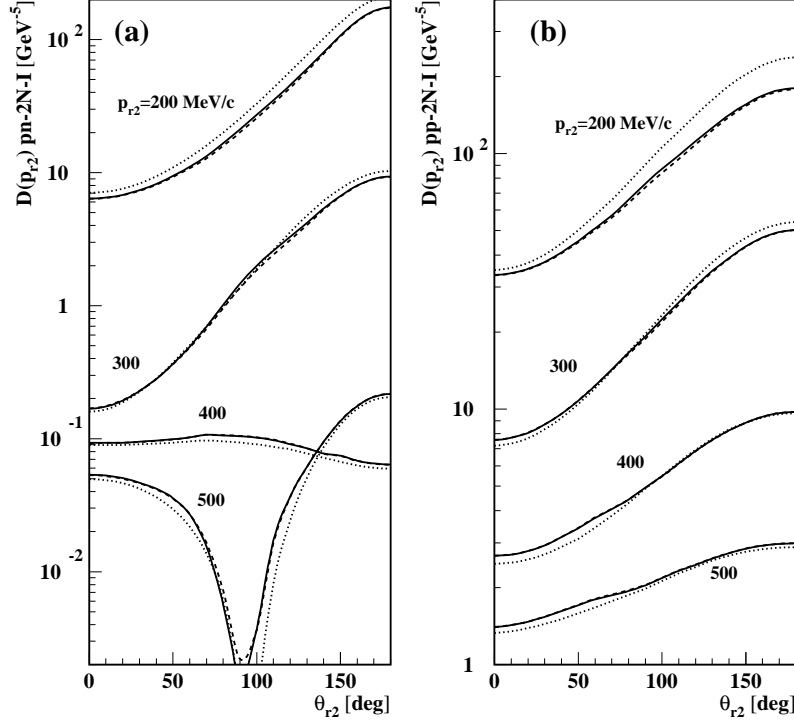

FIG. 19. Dependence of the decay function on the angle of the detected recoil nucleon, θ_{r2} with respect to $\mathbf{q}$ for different and fixed values of p_{r2}. The decay function is calculated for type 2N-II SRC kinematics with missing momentum fixed at $p_m = 100$ MeV/c and $\theta_m = 0^0$. (a) – $(N_f, N_{r2}) \equiv (n,p)$, (b)– $(N_f, N_{r2}) \equiv (p,p)$. Dotted lines - IA, dashed lines - IA+FSI1, solid line - IA+FSI.

Comparison of type 2N-I and 2N-II correlation cases demonstrate that type 2N-II makes the best case for probing the node of the relative momentum distribution in the pp pair in the ^3He wave function (see Figs.19(a) and 20(b)). However, a definitive answer on whether the node can be observed in the experiment requires a careful accounting of non-pole effects in the pair-distortion contribution. This consideration is out of scope of present paper and a dedicated study of the node effects will be presented elsewhere [22].

As in the case of type 2N-I correlations, the effects of double rescattering are marginal which indicates again the feasibility of isolating two-body effects without complication, due to double rescattering of knocked-out nucleon off both recoil nucleons.

C. Type 3N-I Correlations:

A consideration of the angular dependence of the decay function for type 3N-I correlations in Fig.21 reveals a significant effect of FSIs for almost all angles of pair production (or θ_m). The FSI dominates especially at transverse kinematics at $\alpha_m = 1$ which reveals a significant contribution from the double rescattering processes starting at $p_m \geq 400$ MeV/c.

Production of pp pairs (Fig.21(a)) in parallel kinematics provides the best condition for probing type 3N-I SRCs (albeit not without considerable pair distortion effects) starting at $p_m \geq 600$ MeV/c. This can be understood qualitatively. Since each rescattering transfers $k_z \approx \Delta, k_t \leq 500$ MeV/c momentum (predominantly in transverse direction; $k_t > \Delta$), and the rescattering amplitude falls exponentially with k_t^2, it is kinematically infeasible to rescatter two nucleons above 600 MeV/c in the backward direction.
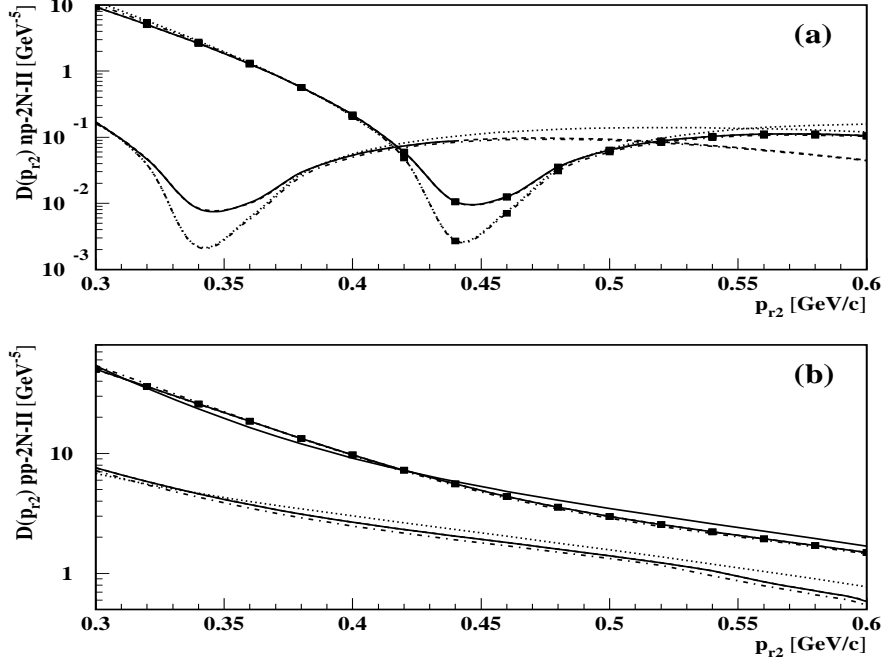
FIG. 20. Dependence of the decay function on the momentum of recoil nucleon, p_{r2} calculated for the kinematics of type 2N-II correlations with missing momentum fixed at $p_m = 100$ MeV/c and $\theta_m = 0^0$. (a) $- (N_f, N_{r2}) \equiv (n,p)$ and (b)$- (N_f, N_{r2}) \equiv (p,p)$. Doted lines - IA prediction, dashed and solid lines for IA+FSI1 and IA+FSI predictions respectively for $\theta_{r2} = 0^0$ kinematics. Curves with square labels corresponds to IA+FSI1 and IA+FSI predictions for anti-parallel $\theta_{r2} = 180^0$ kinematics.

The effects discussed in the previous paragraph can be seen in more detail in the momentum distribution in Fig.22 which confirms again that the only reasonable chance to extract the original momentum distribution in type 3N-I correlation is to measure the coherent recoil pp pair production in the parallel kinematics $\theta_m = 0^0$. Note that the significant contribution from double rescattering processes at transverse kinematics can be also understood qualitatively. To produce two coherent nucleons at large angle it is more preferable for the knocked-out nucleon to scatter consecutively off spectator nucleons. It contributes maximally in the transverse kinematics due to the eikonal nature of NN rescattering which dominates at $\alpha_m = 1$. This situation is reminiscent of the dynamics relevant to the form-factors of few-body systems measured in high momentum transfer reactions, in which case one needs significant rescatterings between constituents of the system to produce coherent combination of the subsystem.
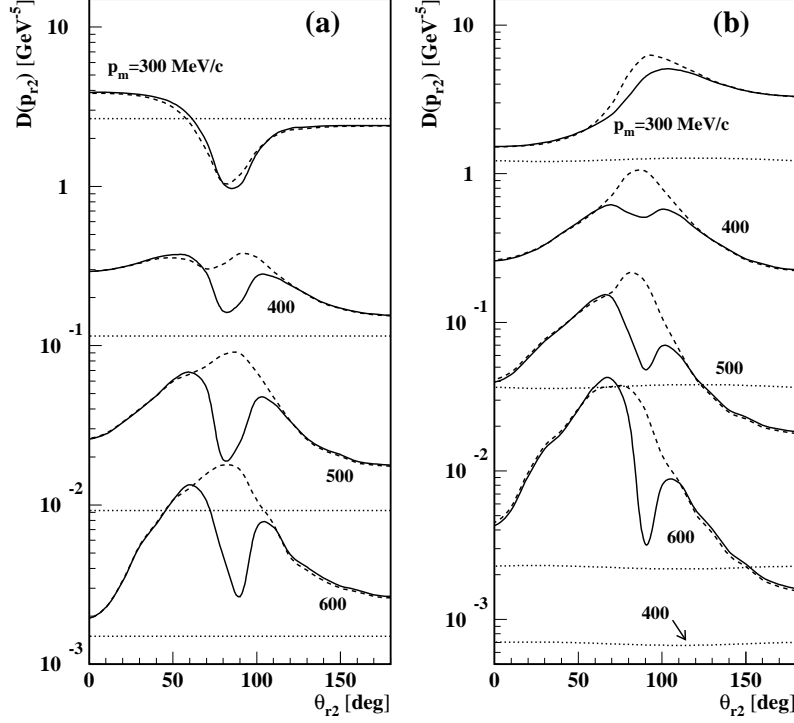
FIG. 21. Dependence of the decay function on the angle of the detected recoil nucleon, θ_{r2}, with respect to $\mathbf{q}$ for different and fixed values of p_m. The decay function is calculated for type 3N-I SRC kinematics such that the recoil momentum of the detected nucleon is opposite to the missing momentum direction and defined as $p_{r2} = \frac{p_m}{2} + 50$ MeV/c. (a) $- (N_f, N_{r2}) \equiv (n,p)$, (b)$- (N_f, N_{r2}) \equiv (p,p)$. Dotted lines - IA, dashed lines - IA+FSI1, solid line - IA+FSI.

D. Type 3N-II Correlations:

In considering the angular dependence of the decay function for type 3N-II correlations in Fig.23, we observe overall large FSI effects except in the kinematics in which both recoil nucleons are produced in the backward direction compared to that of $\mathbf{q}$. In this figure this corresponds to the situation when the recoil nucleon with momentum p_{r2} is produced at $\theta_{r2} = 120^0$ and the fast nucleon is knocked out in parallel kinematics ($\theta_m = 0^0$). This automatically puts the production angle of the second recoil nucleon at $\theta_{r3} = 120^0$ in the other half of the scattering plane.

One can understand the suppression of FSI in this kinematics qualitatively. It is very improbable with one single rescattering to produce two nucleons in the backward hemisphere of knocked-out energetic nucleon. One may expect that double rescattering can contribute to production of such configurations. However, as it will be discussed in the next section, it is dominant only at $\alpha_{r2} \approx \alpha_{r3} \approx 1$ which is significantly away from the considered kinematics. Note that the different angular dependence for recoil pp (a) and pn (b) pairs at momentum range $300 - 500$ MeV/c is related to the qualitative difference in the relative momentum distribution of these pairs (namely to an existing node in pp distribution). Note that recoil nucleon angles $110 < \theta_{r2} < 130$ at $\theta_m = 0^0$ and $p_{r2} = 600$ MeV/c are kinematically forbidden

since in this case $\alpha_m + \alpha_{r2} + \alpha_{r3} \geq 3$. However, the 600 MeV/c curve shows that the FSI is small at broader angular ranges starting at 80^0 to 150^0. This may be very important for probing larger internal momenta in type 3N-II SRCs without substantial FSI effects.
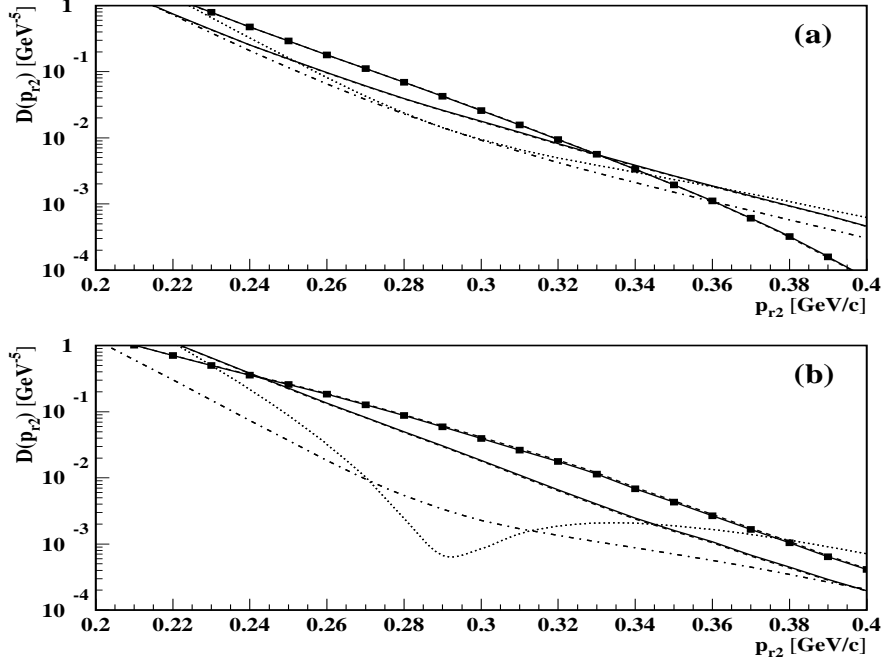

FIG. 22. Dependence of the decay function on the momentum of recoil nucleon, p_{r2}, calculated for the kinematics of type 3N-I correlations. The relation between missing and recoil momenta are the same as in Fig.21. (a) – $(N_f, N_{r2}) \equiv (n, p)$ and (b)– $(N_f, N_{r2}) \equiv (p, p)$. Dotted lines - IA prediction, dashed and solid lines for IA+FSI1 and IA+FSI predictions respectively for $\theta_{r2} = 180^0$ kinematics. Curves with square labels corresponds to IA+FSI1 and IA+FSI predictions for anti-parallel $\theta_{r2} = 0^0$ kinematics.

The momentum distribution of the decay function in Fig.24 confirms the observed, in Fig.23, smallness of FSIs at parallel kinematics with two recoil nucleons produced in the backward hemisphere at 120^0. This situation provides a unique window for accessing type 3N-II correlations. They will be discussed in more details in Sec.IV B 4.

In Fig.24 we also compare the momentum distribution for anti-parallel ($\theta_m = 180^0$) kinematics when recoil nucleons are produced in forward 60^0 angles. Here we observe significant FSIs which enhances the cross section by almost an order of magnitude.

3. Double Rescattering Effects

Previous considerations demonstrated that in practically all cases the maximal FSI is generated in kinematics in which $\alpha_m = 1$. To enhance the effects of double rescattering, relative to the single rescattering contribution, the strategy is to keep $\alpha_m = 1$ and choose kinematics in which two recoil nucleons are produced in symmetric and transverse kinematics. Such configurations boost the double rescattering effects, since in these cases the most economic way to produce two recoil nucleons with large transverse momentum is to

29

have two consecutive rescatterings of the knocked-out nucleon off the spectator nucleons in ^3He. One such kinematics corresponds to the type 3N-I correlations, in which two recoil nucleons are produced with almost vanishing relative momentum. Fig.21 demonstrates a large contribution to double rescattering when two coherent recoil nucleons are produced at almost transverse angles with respect to the direction of **q**.
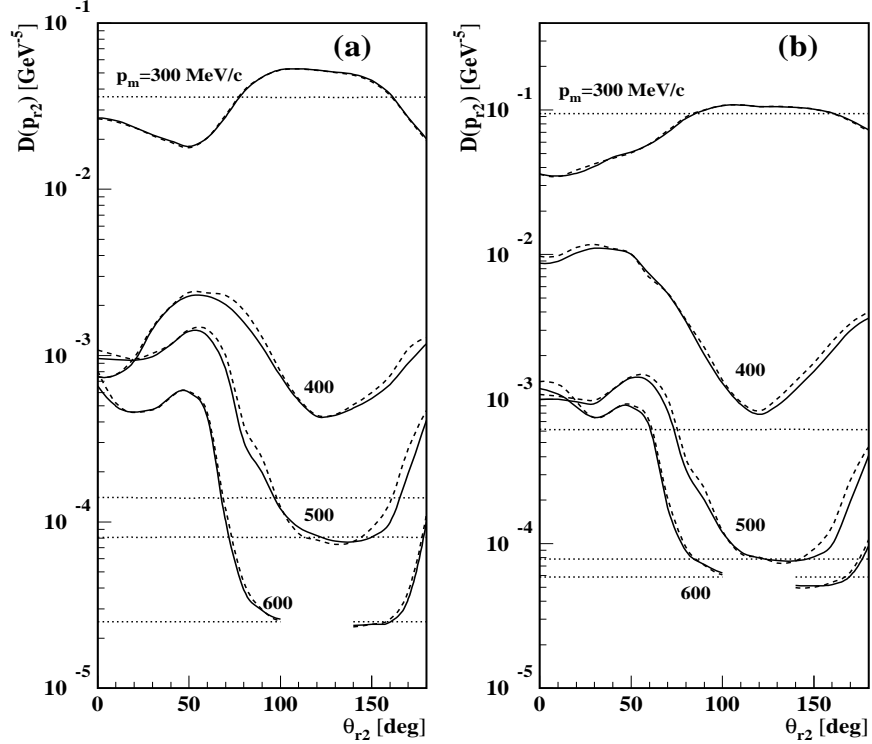

FIG. 23. Dependence of the decay function on the angle of the detected recoil nucleon, θ_{r2}, with respect to **q** for different and fixed values of p_{r2}. The decay function is calculated for type 3N-II SRC kinematics such that $p_m = p_{r2} = p_{r3}$ and relative angles between these momentum vectors are 120^0. Here, $\theta_{r2} = 120^0$ corresponds to $\theta_m = 0^0$. (a) $- (N_f, N_{r2}) \equiv (n, p)$, (b)$- (N_f, N_{r2}) \equiv (p, p)$. Dotted lines - IA, dashed lines - IA+FSI1, solid line - IA+FSI.

In Fig.25 we consider further the kinematics of the type 3N-I correlation by calculating the p_m dependence of the decay function at $\alpha_m = 1$. The result is the significant enhancement of the double rescattering effects starting at $p_m \geq 300$ MeV/c. In the range of $300 \leq p_m \leq 700$ MeV/c, double rescattering screens the single rescattering contribution through its destructive interference with the single rescattering amplitude (see Eqs.(21) and (27) in Ref. [1]). However, starting with $p_m \geq 700$ MeV/c, our calculations show that the decay function is determined predominantly by the square of the double rescattering amplitude of Eq.(27) in Ref. [1]. Since the internal nucleon momenta in the ^3He wave function are small in the double rescattering amplitude, the relativistic effects are expected to be small in spite of $p_m > 700$ MeV/c.
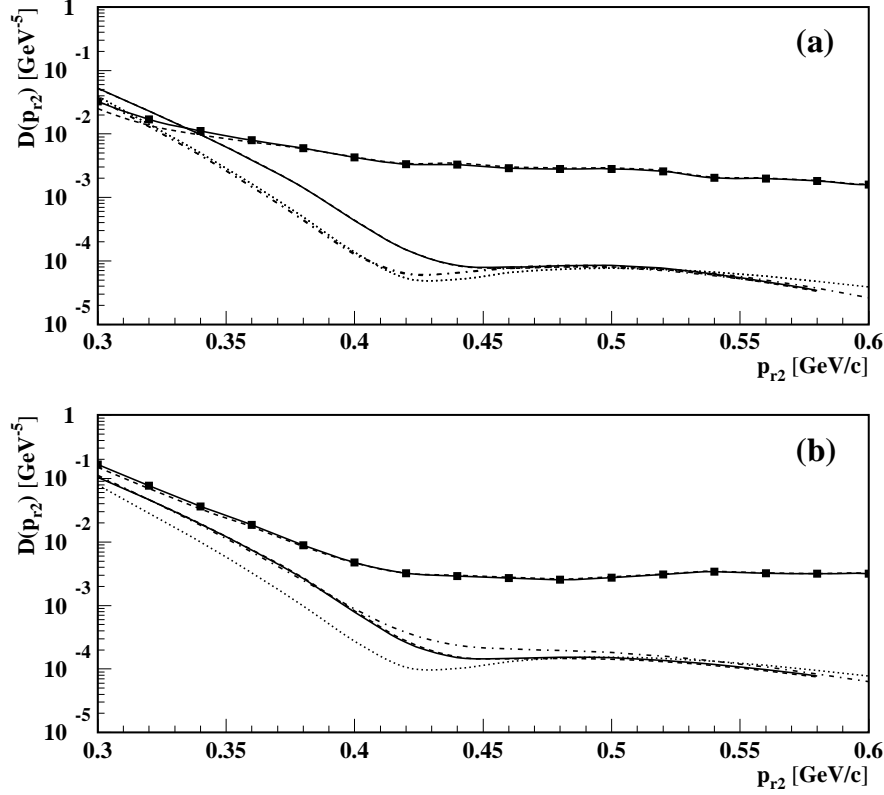
30

FIG. 24. Dependence of the decay function on the momentum of the recoil nucleon, p_{r2}, calculated for the kinematics of type 3N-II correlations. The relation between missing and recoil momenta is the same as in Fig.23. (a) – $(N_f, N_{r2}) \equiv (n, p)$ and (b)– $(N_f, N_{r2}) \equiv (p, p)$. Doted lines - IA prediction, dashed and solid lines for IA+FSI1 and IA+FSI predictions respectively for $\theta_m = 0^0$ ($\theta_{r2} = 120^0$) kinematics. Curves with square labels correspond to IA+FSI1 and IA+FSI predictions for anti-parallel $\theta_m = 180^0$ ($\theta_{r2} = 60^0$) kinematics.

Another kinematical region which provides the symmetric configuration for recoil nucleons is the one close to the type 3N-II correlations in which the light cone momentum fractions of all three nucleons are chosen $\alpha_m = \alpha_{r2} = \alpha_{r3} = 1$, and two recoil nucleons are produced in the opposite halves of the scattering plane. In this case, one again expects the enhanced contribution from double rescattering. The analysis of single (Eq.(21) in Ref. [1]) and double rescattering (Eq.(27) in Ref. [1]) amplitudes shows that the double rescattering contribution is maximized in the kinematics where the interference of single and IA (Eq.(11) in Ref. [1]) amplitudes cancel the square of the single rescattering amplitudes, which happens at $p_m \approx 300$ MeV/c. This can be seen in Fig.26 which displays missing momentum dependence of the decay function in the above kinematical region discussed above. One observes that at $p_m \approx 300$ MeV/c the double rescattering diagram is dominant. It is interesting to note that in this case the dominant part comes from the interference between IA (Eq.(11) in Ref. [1]) and double (Eq.(27) in Ref. [1]) rescattering amplitudes.
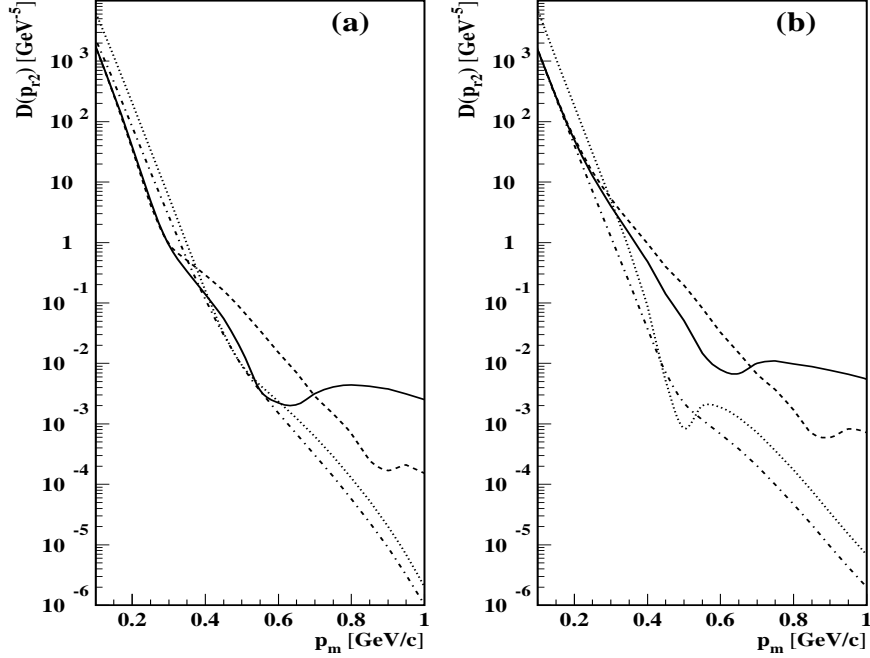
FIG. 25. Dependence of the decay function on p_m at $\alpha_m = 1$ for type 3N-I kinematics. The direction of the recoil nucleons momenta is opposite to that of the missing momentum direction with $p_{r2} = \frac{p_m}{2} + 50$ MeV/c. (a) – $(N_f, N_{r2}) \equiv (n,p)$ and (b)– $(N_f, N_{r2}) \equiv (p,p)$. Dotted line – PWIA, dash-doted – IA, dashed – IA+FSI1 and solid – IA+FSI predictions.

Digression: Color Transparency: The ability to isolate the double rescattering contribution in ^3He electro-disintegration may play a significant role in the ongoing studies of color transparency (CT) phenomena. The main premise of CT is that at sufficiently large Q^2 the knocked-out nucleon is produced in a point like configuration (PLC) which, due to the color neutrality of the object, will have a reduced hadronic interaction strength. Thus, CT phenomena will be manifest in the decreasing of the f_{PLC-N} amplitude of rescattering with an increase of Q^2. This is in contrast to the Q^2 independence of f_{NN} in eikonal approximation.

Presently, two complementary experimental approaches are used to find the signatures for CT phenomenon. One is the attenuation experiments [23] in which nuclear transparency is measured in $(e, e'N)$ reaction off nuclei with $A \geq 2$ and the other is the deuteron electro-disintegration reactions [24] which are aimed at measuring the single rescattering terms in $d(e, e'N)N$ reactions. While attenuation experiments are sensitive to $\sim f_{PLC-N}$, the single-rescattering experiments can provide sensitivity up to $\sim f_{PLC-N}^2$. The possibility of isolating the double rescattering term in ^3He electro-disintegration will allow us to gain unprecedented sensitivity - up to $\sim f_{PLC,N}^4$ (see Eq.(27) in Ref. [1]). Furthermore, isolating the double rescattering amplitude will allow us to address such an intricate questions as whether the first rescattering will destroy the PLC coherence formed by the initial high Q^2 γ^*N scattering.
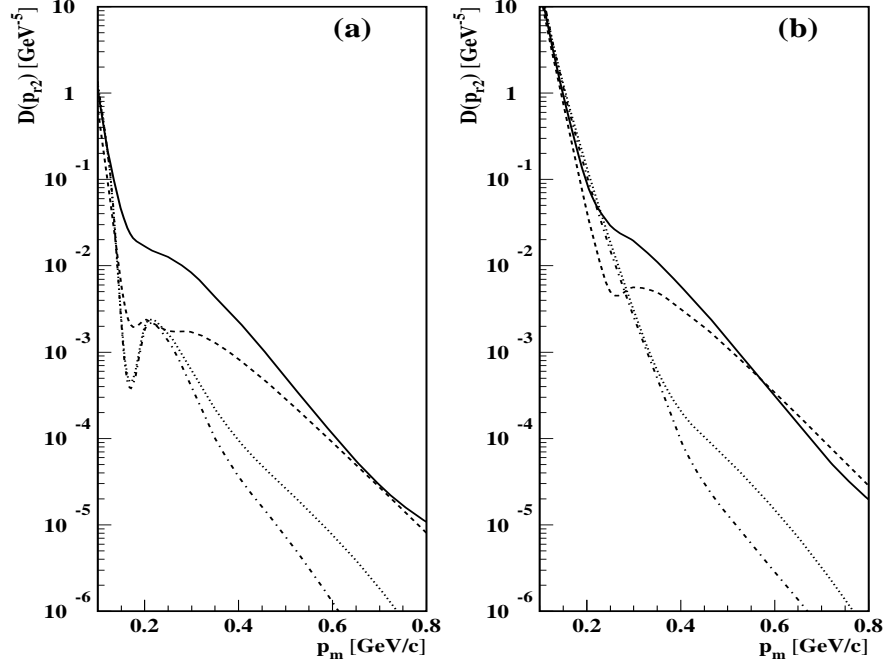
FIG. 26. Dependence of the decay function on p_m at $\alpha_m = \alpha_{r2} = \alpha_{r3} = 1$. (a) – $(N_f, N_{r2}) \equiv (n, p)$ and (b)– $(N_f, N_{r2}) \equiv (p, p)$. Dotted line – PWIA, dash-doted – IA, dashed – IA+FSI1 and solid – IA+FSI predictions.

4. Probing Three Nucleon Forces

Three nucleon forces (3NFs) are one of the most elusive features in nuclear physics. The existence of them for the triton was assumed for the first time by Wigner [25] even before the triton was discovered experimentally. There is little theoretical guidance for systematic building of 3NFs and the main experimental evidence used to constraint the different 3NF models is the binding energy of $A = 3$ nuclei (for review of the present status of 3NFs see [26]). The importance of 3NFs was emphasized in the studies of the binding energies of $A = 3$ nuclei. Furthermore, it allowed for improvements in the calculation of binding energies of nuclei $A = 4 - 9$ [27]. The 3NFs can significantly modify the present models of equations of state of nuclear matter [28], therefore, understanding 3NFs can have a significant impact on our understanding of the physics relevant to the superdense nuclear matter such as neutron stars. However, as it is mentioned in Ref. [26], an accuracy of 1% in calculations are needed in order to systematically disentangle 3NFs forces from the overwhelming 2N interactions in few nucleon systems.

In our consideration of 3NFs, we proceed from the assumption that, just by the nature of 3N forces, they will dominate in type 3N-II correlations. Conversely, in the case of the type 2N-I correlations, it is possible to suppress 3NFs significantly by restricting the momentum of the third spectator nucleon to be close to the zero. Thus, our expectation is that one should observe significantly different contributions from 3NFs in 3N-II and 2N-I correlations. Furthermore, we recall our discussions of type 2N-I and 3N-II correlations in Secs.V.B(2A)

33

and V.B(2D) where we found that one can significantly suppress FSI effects in type 2N-I correlations in parallel kinematics ($\theta_m = 0^0$) (see Fig.18) and in type 3N-II correlations in kinematics where we choose two recoil nucleons to be produced in the backward hemisphere with respect to $\mathbf{q}$ (see Fig.24).
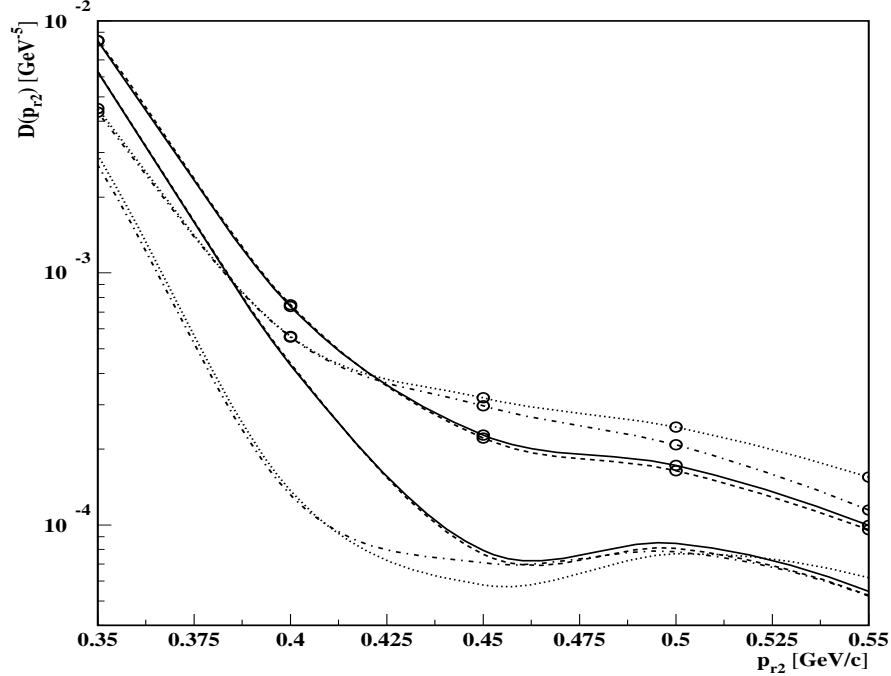

FIG. 27. Dependence of the decay function on the momentum of the recoil nucleon, p_{r2}, calculated for the kinematics of type 3N-II correlations and $(N_f, N_{r2}) \equiv (n, p)$. The relation between missing and recoil momenta is the same as in Fig.23, and the $r2$ recoil proton is detected at $\theta_{r2} = 120^0$ while the angle of missing momentum $\theta_m = 0^0$. Dotted line – PWIA, dash-doted – IA, dashed – IA+FSI1 and solid – IA+FSI predictions. Curves with square labels correspond to the same contributions with three-nucleon forces included in the calculation of the ^3He wave function.

Thus we expect that these kinematic windows are optimal for probing 3NFs. To quantify our statement, in Fig.27 we compare the momentum distributions of the decay function calculated in the type 3N-II kinematics when two recoil protons are produced at 120^0 relative to the $\mathbf{q}$. Calculations are done for two cases: in one case we have only NN interactions while in the other case 3NFs are included according to the Tucson-Melbourne model [29]. Our calculations show a factor of two difference between calculations including only 2N forces and calculation including 2N+3NF forces.

In contrast, the calculations in the kinematics of the type 2N-I correlations presented in Fig.28, using the same two models of NN interactions, predict little difference between momentum dependences of the decay function.

These considerations show that we can identify the domains in the kinematics of type 3N-II correlations where FSI effects are relatively small and one has a good chance to extract the genuine information about 3NFs. This assumes one is doing simultaneous measurement also in 2N-I kinematics where the same 3NFs will give a negligible contribution.
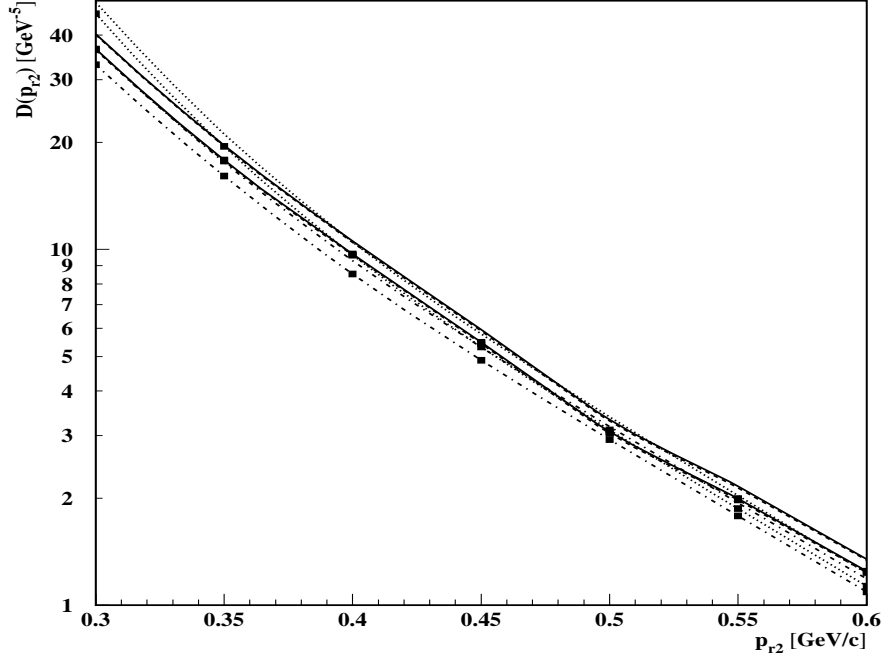
34

FIG. 28. Dependence of the decay function on the momentum of the recoil nucleon, p_{r2}, for type 2N-I kinematics at $\theta_{r2} = 180^0$ ($\theta_m = 0^0$). $(N_f, N_{r2}) \equiv (n, p)$. Dotted line – PWIA, dash-doted – IA, dashed – IA+FSI1 and solid – IA+FSI predictions. Curves with circular labels correspond to the same contributions with three-nucleon forces included in the calculation of the ^3He wave function.

V. SUMMARY

Based on generalized eikonal approximation, developed in the part-I of this work [1], for high Q^2 electro-disintegration of $A = 3$ system we perform numerical studies of exclusive $^3He(e, e'N)NN$ reactions.

As an input, in our numerical studies we use: (i) The Bochum group's [11] calculation of ground state ^3He wave function for different sets of realistic NN interaction potentials as well as calculations which explicitly include three nucleon forces in the ground state. (ii) The SAID group's [12] parameterization of low-to-intermediate energy NN scattering amplitudes to calculate the two-nucleon continuum state wave function which is needed in order to evaluate the interaction between recoil nucleons in the final state of the reaction (pair distortion effects). (iii) We use our updated parameterization of high energy NN scattering amplitudes in the calculation of the small angle rescattering of struck nucleon off spectator nucleons [13].

To describe the exclusive $^3He(e, e'N)NN$ reaction we use the formalism of the decay function which is related to the conventional spectral function through the integration of the phase space of the recoil nucleons.

In the numerical analyses of both spectral and decay functions, we concentrate on studies of two main types of 2N and 3N correlations. For 2N correlations, we consider the ones in

35

which the struck nucleon is initially correlated with one of the recoil nucleons while the third nucleon is spatially isolated (type 2N-I SRC). Also for the case of 2N correlations we consider the case in which the two recoil nucleons are in 2N correlation with the struck nucleon in the mean field of the SRC pair (type 2N-II SRC). For 3N correlations we consider the correlations in which struck nucleon with large missing momenta is correlated with the pair of coherent nucleons (type 3N-I SRC). For the 3N correlations we also consider the case in which all three nucleons have relative momenta exceeding the characteristic mean field momentum in the nucleus and have a relative angle $\approx 120^0$ (type 3N-II SRC).

In discussing the spectral function, we demonstrate that it exhibits several unique features related to the structure of 2N correlations. These are the correlation between missing momenta and missing energy and the minimum in the spectral function associated with the node in the relative momentum distribution of the pp pair. These results are in agreement with previous analyzes of spectral function (see e.g. [15]). There are, however, no clear cut signatures in the spectral function related to the 3N correlations. Within PWIA, 3N SRCs reveal only through the strength of spectral function at very high values of missing momenta and/or energy. Our new result in considering the spectral function is that the strength related to the 3N SRCs is practically washed out by the pair distortion and the FSI effects.

Considering the decay function, which is practically an unexplored quantity, we observe that within PWIA it clearly exhibits the main features of 2N and 3N correlations. Subsequent analysis of pair distortion and FSI effects revealed that the additional degrees of freedom associated with the full detection of the decay products of the reaction allows us to pinpoint unambiguously the kinematics in which the FSI or SRC plays a dominant role. Our conclusion is that the comprehensive study of the decay function in exclusive reactions will allow an unprecedented access to the 2N and 3N correlations in the nuclei.

We highlight two particular cases. One is the possibility to isolate double rescattering effects which can provide us a new and powerful tool in studying color transparency phenomena. The other is identifying a kinematic window that will allow us to probe directly the effects associated with three-nucleon forces in the ground state wave function of ^3He.

Our overall conclusion is that the investigation of the decay function opens up a completely new venue in studies of short range nuclear properties and allows us to discriminate between different orders of final state reinteractions. The latter will provide a powerful tool in studies of color transparency phenomena.

ACKNOWLEDGMENTS

REFERENCES

[1] M.M. Sargsian, T.V. Abrahamyan, M.I. Strikman, L.L. Frankfurt, *Exclusive Electro-Disintegration of ^3He at high Q^2: I. Generalized Eikonal Approximation*, Part-I, arXiv:nucl-th/0406020, Phys. Rev. **C** (*in press*).

[2] L.L. Frankfurt, M.M. Sargsian and M.I. Strikman, Phys. Rev. **C56** (1997) 1124.

[3] M. M. Sargsian, Int. J. Mod. Phys. E **10**, 405 (2001).

[4] L.L. Frankfurt, J.A. Miller and M.I. Strikman, *Ann. Rev. Nucl. Part. Sci.* **44**, 501 (1994).

[5] C. Ciofi degli Atti and L. P. Kaptari, Phys. Rev. C **66**, 044004 (2002).

[6] L.L. Frankfurt and M.I. Strikman, Phys. Rep. **160**, 235 (1988).

[7] T. De Forest, Nucl. Phys. A **392**, 232 (1983).

[8] G. Bizard *et al.*, Nucl. Phys. B **85**, 14 (1975); M. N. Kreisler *et al.*, Nucl. Phys. B **84**, 3 (1975); E. L. Miller *et al.*, Phys. Rev. Lett. **26**, 984 (1971).

[9] Y. I. Azimov, Sov.Phys. JETP, v.16, 1640 (1963); Phys.Lett., v.3, 195 (1963).

[10] W. R. Gibbs and B. Loiseau, Phys. Rev. C **50**, 2742 (1994).

[11] A. Nogga A. Kievsky, H. Kamada, W. Gloeckle, L. E. Marcucci, S. Rosati and M. Viviani, Phys. Rev. C **67**, 034004 (2003).

[12] R. A. Arndt, I. I. Strakovsky and R. L. Workman, Phys. Rev. C **62** (2000) 034005.

[13] T.V. Abrahamyan, *Master's Thesis*, unpublished, FIU, 2003.

[14] R. B. Wiringa, V. G. J. Stoks and R. Schiavilla, Phys. Rev. C **51**, 38 (1995)

[15] C. Ciofi degli Atti, L. P. Kaptari and D. Treleani, Phys. Rev. C **63**, 044601 (2001)

[16] L.L. Frankfurt and M.I. Strikman, Phys. Rept. **76**, 215 (1981).

[17] C. Ciofi degli Atti, S. Simula, L. L. Frankfurt and M. I. Strikman, Phys. Rev. C **44**, 7 (1991).

[18] C. Marchand *et al.*, Phys. Rev. Lett. **60**, 1703 (1988).

[19] D. L. Groep *et al.*, Phys. Rev. C **63**, 014005 (2001).

[20] L.L. Frankfurt, W.R. Greenberg, G.A. Miller, M.M. Sargsian and M.I. Strikman, Z.Phys. **A352**, 97 (1995).

[21] R. A. Niyazov and L. B. Weinstein [CLAS Collaboration], Phys. Rev. Lett. **92**, 052303 (2004)

[22] T. Abrahamyan and M. Sargsian *in preparation*.

[23] K. Garrow *et al.*, Phys. Rev. C **66**, 044613 (2002). *Jefferson Lab Proposal E94-102*, 1994.

[24] K. Sh. Egiyan, K. A. Griffioen and M.I. Strikman(spokespersons) 1994 Measuring Nuclear Transparency in Double Rescattering Processes, *Jefferson Lab Proposal E94-019*, 1994.

[25] E. Wigner, Phys. Rev. **43**, 252 (1933).

[26] J. L. Friar, Nucl. Phys. A **684**, 200 (2001).

[27] S. C. Pieper, V. R. Pandharipande, R. B. Wiringa and J. Carlson, Phys. Rev. C **64**, 014001 (2001).

[28] H. Heiselberg and V. Pandharipande, Ann. Rev. Nucl. Part. Sci. **50**, 481 (2000).

[29] S. A. Coon and H. K. Han, Few Body Syst. **30**, 131 (2001).